

Symmetry-based theory of Dirac fermions on two-dimensional hyperbolic crystals: Coupling to the spin connection

Ana Djordjević,¹ Marija Dimitrijević Ćirić,¹ and Vladimir Juričić^{2,*}

¹*Faculty of Physics, University of Belgrade, Studentski Trg 12-16, 11000 Belgrade, Serbia*

²*Departamento de Física, Universidad Técnica Federico Santa María, Casilla 110, Valparaíso, Chile*

(Dated: July 14, 2025)

Discrete fermionic and bosonic models for hyperbolic lattices have attracted significant attention across a range of fields since the experimental realization of hyperbolic lattices in metamaterial platforms, sparking the development of hyperbolic crystallography. However, a fundamental and experimentally consequential aspect remains unaddressed: fermions propagating in curved space inherently couple to the underlying geometry via the spin connection, as required by general covariance—a feature not yet incorporated in studies of hyperbolic crystals. Here, we introduce a symmetry-based framework for Dirac fermions on two-dimensional hyperbolic lattices, explicitly incorporating spin-curvature coupling via a discrete spin connection. Starting from the continuous symmetries of the Poincaré disk, we classify the irreducible representations and construct a symmetry-adapted basis, establishing a direct correspondence to the continuum Dirac theory. We show that this continuum theory predicts a finite density of states at zero energy for any finite curvature in D -dimensional hyperbolic space with $2 \leq D \leq 4$, suggesting enhanced susceptibility of Dirac fermions to interaction-driven instabilities at weak coupling. We then derive explicit forms of discrete translational and rotational symmetries for lattices characterized by Schläfli symbols $\{p, q\}$, and explicitly construct the discrete spin connection, represented as local hopping phases, via parallel transport. Our results pave the way for experimental realization of spin-curvature effects in metamaterial platforms and systematic numerical studies of correlated Dirac phases in hyperbolic geometries.

Contents			
I. Introduction	1	C. Noncommutativity of translations	18
A. Key results	2	D. Dirac equation in hyperbolic space	19
B. Organization	2	1. Dirac equation in flat space	20
II. Geometry of the Poincaré disk: Isometries and their irreducible representations	3	E. Symmetries of the Dirac equation on the Poincaré disk	21
A. Killing vectors	3	F. Parallel transport method for discrete spin connection	21
B. Irreducible representations	4	References	23
C. Spinors on the Poincaré disk	6		
D. Density of states	6		
III. Discretization of Poincaré disk	8		
A. Point group symmetry	9		
B. Translations	11		
IV. Construction of the discrete spin connection	12		
A. Discrete spin connection in the zeroth generation polygons	13		
B. Discrete spin connection on the polygons in farther generations	13		
V. Conclusions and outlook	15		
A. Coordinate transformation and geodesics	16		
B. Point group discretization	17		

I. Introduction

The renowned anti-de Sitter/conformal field theory (AdS/CFT) correspondence [1–3] has driven extensive research into quantum field theory in hyperbolic space. At the same time, studies in holography and quantum information theory have revealed deep connections between geometry, entanglement, and renormalization [4–8]. These theoretical advances have been complemented by experimental progress, enabling the simulation of negatively curved space-time in controlled settings.

One promising approach employs hyperbolic metamaterials, where spatial variations in the dielectric constant effectively encode the effects of curvature [9–15]. Other platforms for realizing the Dirac equation in curved space-time have been proposed, including ion traps [16, 17], optical waveguides [18], and optical lattices with position-dependent hopping and non-Abelian artificial gauge fields [19]. Building on these developments,

* Corresponding author:vladimir.juricic@usm.cl

recent progress in quantum electrodynamics, superconducting microwave resonator networks [20], and topoelectric circuits [21–24] has further expanded the capabilities for simulating lattice models and conformal field theories in hyperbolic space, which also play a key role in the emerging field of hyperbolic crystallography [25–31].

Hyperbolic crystals are regular tessellations of hyperbolic space generalizing the notion of the crystal in the Euclidean (flat) space to its negatively curved counterpart with a constant curvature where the tiling is realized by polygons of p sides forming a network of sites (vertices) with the q nearest neighbors. Such a lattice structure is commonly denoted by Schläfli symbols $\{p, q\}$, with the regular hyperbolic space tessellation achieved when $(p - 2)(q - 2) > 4$ giving rise to a much richer structural landscape than in the Euclidean space where the condition $(p - 2)(q - 2) = 4$ yields only three possible regular tessellations corresponding to square $\{4, 4\}$, triangular $\{3, 6\}$, and honeycomb $\{6, 3\}$ lattices. To elegantly embed the $\{p, q\}$ -hyperbolic lattice into the continuum hyperbolic space—and thereby capture the continuum limit, a key element of our analysis—we employ the Poincaré disk.

The study of band structures in hyperbolic crystals has been developed within the framework of hyperbolic band theory [25–29], which extends the conventional Bloch theorem to negatively curved space. Notably, hyperbolic analogs of topological phases [32–40] have been explored, demonstrating that bulk topological invariants and protected edge modes remain well-defined in hyperbolic space. Moreover, the concept of topological band nodes has been generalized to negatively curved geometries [41], with a corresponding linear scaling of the density of states (DOS) found for lattices where $p/2$ is an odd integer [42]. Beyond these topological aspects, a variety of condensed matter phenomena have been investigated in hyperbolic systems, including Hofstadter spectra [43, 44], flat bands [45–48], strong correlation effects [42, 49–52], non-Hermitian phenomena [53–55], and fracton physics [56, 57]. However, existing tight-binding models for fermions on hyperbolic lattices entirely neglect spin, resulting in an effective description where fermions behave effectively as scalar bosons in terms of their band structure properties, with this limitation remaining a key challenge in the studies of hyperbolic materials thereby paving the way for exciting future research.

From the point of view of gravity, there is a fundamental difference between the fermions and scalar bosonic particles. The former “feel” the curvature through the spin connection that couples geometry to the particles’ spin, while for the latter this is not the case (technically, the covariant derivative for a scalar is just an ordinary partial derivative) [58]. However, to the best of our knowledge, the explicit coupling of the electron spin to the curvature through the spin connection, here referred to as spin-curvature coupling, in the lattice models implemented on the hyperbolic crystals has not been accounted for so far, but should yield nontrivial effects, such as a

finite density of states at zero energy for Dirac fermions, and thereby curvature-induced quantum phase transitions for weak electron-electron interactions. Indeed, this feature may be expected based on the engineering scaling dimension of the DOS being $D - 1$, $[\rho] = D - 1$ for the Dirac fermions in D spatial dimensions, and the fact that for the scalar curvature $[R] = -2$ in units of the inverse length, implying that the zero-energy DOS in D spatial dimensions scales with curvature as $\rho \sim |R|^{(D-1)/2}$. In turn, this may lead to the dynamic mass generation via the spontaneous symmetry breaking at weak coupling. Other possible consequences of this coupling include the curvature-driven band inversion tuning the transitions into novel topological phases on the curved space background, and realization of long sought pure gravitational anomalies for the electronic systems.

A. Key results

Motivated by these considerations, we systematically incorporate spin-curvature coupling on hyperbolic lattices. To this end, we first analyze the isometries of the Poincaré disk model, which provides the continuum embedding for hyperbolic lattices and thereby determines the symmetry structure of the system. This, in turn, facilitates the construction of spinor fields via the irreducible representations of the projective $SU(1, 1)$ group, $PSU(1, 1)$, explicitly realized through the associated Killing vectors, as detailed in Secs. II B and II C. As we then show, Dirac fermions in this space therefore coupled to the geometry via the spin connection, yield a finite density of states at zero energy for any finite curvature (Sec. II D), with the form $\rho(0) \sim |R|^{(D-1)/2}$, consistent with general scaling arguments, which sheds light on the apparent universality of weak coupling instabilities of Dirac fermions coupled to the hyperbolic space [59]. To construct the discrete form of the spin connection on an arbitrary hyperbolic lattice, as a first step we find the explicit form of the discrete translation and rotational symmetries of the hyperbolic lattice characterized by the Schläfli symbols $\{p, q\}$, given by Eqs. (86) and (100), respectively. Using this result, by employing the approach in Ref. [60] to the hyperbolic space, we finally arrive to the main result of the paper, the form of discrete spin connection, as shown in Sec. IV, which in the continuum limit minimally couples to Dirac fermions.

B. Organization

The paper is organized as follows. In the following Section II, we study geometry of the Poincaré disk model of hyperbolic space, its group symmetry irreducible representation, spinors and density of states. In Section III, we obtain the discrete translation and rotational symmetries of the hyperbolic lattice embedded on the Poincaré disk. The explicit construction of the discrete spin connection

is carried out in Section IV. We summarize our results in Section V and present technical details in Appendices.

II. Geometry of the Poincaré disk: Isometries and their irreducible representations

Understanding the properties of a hyperbolic lattice embedded in the Poincaré disk requires a careful examination of its symmetries, which is crucial when constructing spinors and the corresponding discrete spin connection therein. The Poincaré disk model, defined as $\mathbb{D} = \{z \in \mathbb{C} : |z| < l\}$, represents the hyperbolic plane and is equipped with the metric

$$ds^2 = \frac{dx^2 + dy^2}{(1 - \frac{|z|^2}{l^2})^2}. \quad (1)$$

To uncover the isometries of the Poincaré disk, we take a geometric approach, identifying symmetry generators through Killing vectors, which define the coordinate transformations that preserve the metric in Eq.(1). In turn, such symmetry transformations are indispensable for the construction of irreducible representations carried out in Sec.II B. Furthermore, as embedding spinors in the Poincaré disk can be viewed as the long-wavelength limit of lattice spinors in a discrete hyperbolic lattice, it motivates us to explore the explicit form of the spinors as the solutions of the Dirac equation on the Poincaré disk, as discussed in Sec.II C, and, in particular, to derive the corresponding DOS in Sec.II D.

A. Killing vectors

To set the stage, we first analyze the symmetries of Poincaré disk by identifying its Killing vectors and their algebra, which, at the same time, provides a more transparent geometric picture of its isometries. Using these results, we then determine the coordinate transformations generated by the Killing vectors and derive the geodesics, describing the trajectories of a free particle in this space. To this end, we solve the Killing equation,

$$\partial_\mu \xi_\nu + \partial_\nu \xi_\mu = 2\Gamma_{\mu\nu}^\rho \xi_\rho, \quad (2)$$

which also represents an integral of the geodesic equation. Now, invoking the form of the Christoffel symbols in Eqs. (A1)-(A4) and the metric of the Poincaré disk [Eq. (1)], we find that the Killing equation reduces to the Cauchy-Riemann conditions for the Killing vectors,

$$\partial_x \xi^x = \partial_y \xi^y, \quad (3)$$

$$\partial_x \xi^y = -\partial_y \xi^x, \quad (4)$$

which are therefore equivalent to the Killing equations of the two-dimensional conformal group [61]. Eqs. (3) and (4) then allow to express the isometries of the

Poincaré disk in the form of analytic and anti-analytic functions,

$$\xi = \xi^x + i\xi^y, \quad (5)$$

$$\bar{\xi} = \xi^x - i\xi^y, \quad (6)$$

where the analytic and anti-analytic function are, respectively, given by $\xi = a_{-1} + a_0 z + a_1 z^2$ and $\bar{\xi} = \bar{a}_{-1} + \bar{a}_0 \bar{z} + \bar{a}_1 \bar{z}^2$, with $z = x + iy$. Substituting this *ansatz* into Eq. (2) yields three Killing vectors,

$$\xi_1 = (-l^2 + x^2 - y^2) \partial_x + 2xy \partial_y, \quad (7)$$

$$\xi_2 = -y \partial_x + x \partial_y, \quad (8)$$

$$\xi_3 = 2xy \partial_x + l(-l^2 - x^2 + y^2) \partial_y. \quad (9)$$

Therefore, Killing vector ξ_2 represents the generator of rotations in the plane, i.e., the angular momentum. The other two Killing vectors ξ_1 and ξ_3 can be interpreted as a combination of generators of translations and special conformal transformations. Furthermore, the obtained Killing vectors correspond to the generators of the Virasoro algebra of the conformal group, specifically $\{L_{\pm 1}, L_0, \bar{L}_{\pm 1}, \bar{L}_0\}$, with the identifications,

$$\xi_1 = L_{-1} - L_1 + \bar{L}_{-1} - \bar{L}_1, \quad (10)$$

$$\xi_2 = i(-L_0 + \bar{L}_0), \quad (11)$$

$$\xi_3 = i[(L_{-1} + L_1) - (\bar{L}_{-1} + \bar{L}_1)]. \quad (12)$$

As such, they satisfy the Lie algebra

$$[\xi_1, \xi_2] = \xi_3, \quad (13)$$

$$[\xi_1, \xi_3] = 4\xi_2, \quad (14)$$

$$[\xi_2, \xi_3] = \xi_1, \quad (15)$$

which is isomorphic to the algebra $\mathfrak{sl}(2, \mathbb{R})$, generating the symmetry of Poincaré disk. As a consequence, the corresponding finite coordinate transformations take the form

$$z' = e^{(\bar{a}z^2 + i\theta z - a)\partial} z, \quad (16)$$

with the isometries of the disk \mathbb{D} corresponding conformal automorphisms,

$$z' = e^{i\bar{\theta} \frac{z - c}{1 - \bar{c}z}}, \quad (17)$$

as explicitly demonstrated in App. A. As expected, these transformations are isomorphic to the group $\text{PSL}(2, \mathbb{R})$ of Möbius transformations on the upper half-plane [62].

We use these Killing vectors and conserved quantities to find the equations of geodesic curves in this space,

$$g_{\mu\nu} \frac{dx^\mu}{d\tau} \frac{dx^\nu}{d\tau} = C_4, \quad (18)$$

$$\frac{dx^\mu}{d\tau} \xi_\mu = C, \quad (19)$$

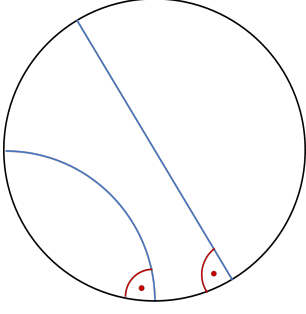


Figure 1. Geodesics on the Poincaré disk. First class of geodesics given by the straight line passes through the center of the disk, and intersects the edges at the angle of $\pi/2$, as given by Eq. (20). Second class of geodesics is represented by circles that do not pass through the center and are orthogonal to the edges, as given by Eq. (21).

where C and C_4 are constants, and τ as the geodesic parameter, which ultimately yield the following geodesic curves:

$$y = Dx, \quad (20)$$

$$(x - x_0)^2 + (y - y_0)^2 = x_0^2 + y_0^2 - l^2, \quad (21)$$

where D , x_0 and y_0 are real constants, and correspond to two distinct classes of geodesics. First, the geodesic line in Eq. (20) describes a particle moving along a straight line crossing the center of the disk \mathbb{D} (Fig. 1), while the ones in Eq. (21) imply that the particle can also follow a circular trajectory orthogonal to the edge circle of the disk lying at infinity, as shown in Fig. 1. See App. A for details. Finally, the distance between two points on the Poincaré disk is

$$d(z, z') = \frac{l}{2} \operatorname{arcosh} \left(1 + \frac{2l^2 |z - z'|^2}{(l^2 - |z|^2)(l^2 - |z'|^2)} \right). \quad (22)$$

Using these results, in the following we find the form of the irreducible representations for the algebra of the isometries $\mathfrak{sl}(2, \mathbb{R})$ given by Eqs. (13)-(15), generating the isometries of Poincaré disk, given by the automorphism in Eq. (17).

B. Irreducible representations

We first notice that the group describing the isometries of the Poincaré disk model is $\mathrm{SL}(2, \mathbb{R}) \cong \mathrm{PSU}(1, 1)$, which is a quotient of the special unitary group $\mathrm{SU}(1, 1)$ by its center $\{\mathbb{I}, -\mathbb{I}\}$, i.e., $\mathrm{SU}(1, 1)$ is the universal cover of the isometry group of the Poincaré disk. The unitary irreducible representations can therefore be determined by employing steps similar to those used to construct the irreducible representations of the $\mathfrak{su}(2) \cong \mathfrak{so}(3)$ algebra, which is generated by the angular momentum operator. To this end, we first compute the Casimir operator of the

$\mathfrak{su}(1, 1)$ algebra

$$\xi^2 = \xi_2^2 - \frac{1}{4}\xi_1^2 - \frac{1}{4}\xi_3^2, \quad (23)$$

which together with ξ_2 form a set of mutually commuting operators, therefore spanning common orthonormal basis,

$$\xi_2 |q, m\rangle = im |q, m\rangle, \quad (24)$$

$$\xi^2 |q, m\rangle = q |q, m\rangle, \quad (25)$$

with the eigenvalue of the Casimir operator being real. We then construct the irreducible representations by determining the conditions on the quantum numbers q and m , the eigenvalues of the operators ξ^2 and ξ_2 , respectively.

To this end, let us first introduce Hermitian-like operators, $\eta_j = -i\xi_j$ ($j = 1, 2, 3$), and therefore $\eta^2 = -\xi^2$. We furthermore choose mutually adjoint operators in the form

$$\eta_{\pm} = \frac{1}{2}(\eta_1 \pm i\eta_3), \quad (26)$$

which together with η_2 span the same space as the three Killing vectors, with the corresponding commutation relations of the form

$$[\eta_2, \eta_{\pm}] = \pm \eta_{\pm}, \quad (27)$$

$$[\eta_+, \eta_-] = 4\eta_2. \quad (28)$$

From the commutation relation in Eq. (27) we obtain

$$\eta_2(\eta_{\pm} |q, m\rangle) = (m \pm 1)(\eta_{\pm} |q, m\rangle), \quad (29)$$

which implies that η_{\pm} can be interpreted as creation and annihilation operators corresponding to the quantum number m . Action of η_+ on a state $|q, m\rangle$ can then be written as

$$\eta_+ |q, m\rangle = \alpha_{q,m}^+ |q, m+1\rangle, \quad (30)$$

with

$$\alpha_{q,m}^+ = \sqrt{m(m+1) - q}. \quad (31)$$

Similarly, for the operator η_- , we find

$$\eta_- |q, m\rangle = \alpha_{q,m}^- |q, m-1\rangle, \quad (32)$$

$$\alpha_{q,m}^- = \sqrt{m(m-1) - q}. \quad (33)$$

Eqs. (30) and (32) imply that the quantum number m can be written as

$$m = \mu + n, \quad (34)$$

where $\mu \in \mathbb{R}/\mathbb{Z}$ and $n \in \mathbb{Z}$. We now analyze the domain of m considering the condition for the coefficients $|\alpha_{q,m}^{\pm}|^2 \geq 0$, which implies that the quantum numbers m and q satisfy

$$m^2 \pm m - q \geq 0, \quad (35)$$

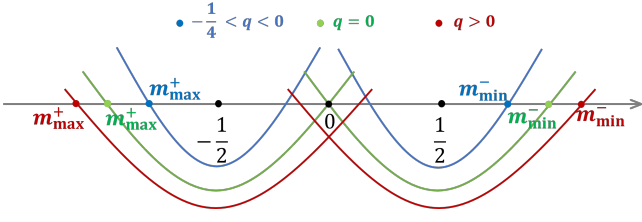


Figure 2. The domains of allowed values for m as a function of q , as given by Eq. (35), where m is represented along the gray axis. Each curve corresponds to the boundaries set by $m^2 \pm m - q = 0$ for different regimes of q . For $q > 0$ (red curve), a gap appears in the allowed values of m . At the critical point $q = 0$ (green curve), this gap closes, while for $q \in [-1/4, 0)$ (blue curve), the spectrum of m becomes fully connected, indicating the absence of any forbidden intervals (gaps).

with $\alpha_{q,m}^\pm$ vanishing when the following conditions are satisfied,

$$m_\pm^\pm = \frac{-1 \pm \sqrt{1+4q}}{2}, \quad (36)$$

$$m_\pm^\mp = \frac{1 \pm \sqrt{1+4q}}{2}, \quad (37)$$

and m^\pm correspond to the solutions for $\alpha_{q,m}^\pm$.

To determine the values of the quantum numbers (q, m) , we analyze the discriminant in Eqs. (36) and (37). Quantum number m being purely real, $m \in \mathbb{R}$, implies that $q \geq -\frac{1}{4}$. The maximal and minimal values (weights) of m^\pm , labeled as m_{\max}^+ and m_{\min}^- , respectively, are defined so that $m_{\max}^+ \equiv m_+^+$ and $m_{\min}^- \equiv m_-^-$. Now the conditions on maximal and minimal weights m_{\max}^+ and m_{\min}^- , respectively, for the different domains of quantum number q , read

$$(i) \quad q \in (0, +\infty) \implies \begin{cases} m_{\max}^+ \in (-\infty, -1), \\ m_{\min}^- \in (1, +\infty), \end{cases} \quad (38)$$

$$(ii) \quad q \in \left[-\frac{1}{4}, 0\right] \implies \begin{cases} m_{\max}^+ \in \left[-1, -\frac{1}{2}\right], \\ m_{\min}^- \in \left[\frac{1}{2}, 1\right]. \end{cases} \quad (39)$$

We then find for the domain (i) [Eq. (38)] that $m \in (-\infty, m_{\max}^+] \cup [m_{\min}^-, +\infty)$, therefore featuring a gap. On

the other hand, the domain (ii) [Eq. (39)] is gapless and there is no restriction on the values of $m = \mu + n$, see Fig. 2.

Note that, in general, the representations of the algebra $\mathfrak{su}(1,1)$ are infinite-dimensional. A special subset of finite-dimensional irreducible representations are obtained by restricting $m \in \mathbb{Z}$, i.e. $\mu = 0$ in Eq. (34), yields a quantization condition for the quantum number q ,

$$q = b(b+1), \quad b \in \mathbb{Z}, \quad (40)$$

where b is defined so that the discriminant is an odd number, $1+4q = (2b+1)^2$. In this case, the maximum and minimum weights of m are given by

$$m_{\max}^+ = -b-1 \wedge m_{\min}^- = b+1, \quad (41)$$

and quantum number m has a gap.

Let us now solve the eigenvalue problem for the set of mutually commuting operators ξ_2 and ξ^2 , Eqs. (24) and (25), in coordinate space. The Casimir operator reads

$$\xi^2 = -\frac{l^2}{4} \Delta_g, \quad (42)$$

where Δ_g is the generalization of Laplace operator in curved space, the Laplace-Beltrami operator, explicitly given by

$$\Delta_g = \left(1 - \frac{|z|^2}{l^2}\right)^2 (\partial_x^2 + \partial_y^2). \quad (43)$$

The eigenvalue problem of the obtained Casimir operator can be cast in the form of the Schrödinger equation in curved space,

$$-\frac{\hbar^2}{2m^*} \Delta_g \Phi_{q,m}(r, \varphi) = \frac{4q\hbar^2}{2m^* l^2} \Phi_{q,m}(r, \varphi), \quad (44)$$

with $\Phi_{q,m}(r, \varphi) = \langle r, \varphi | q, m \rangle$ as the coordinate representation of the symmetry adapted basis. Consequently, we can interpret $\frac{4q\hbar^2}{2m^* l^2}$ as energy, where m^* is the effective mass. Moreover, we can write the eigenvalue q as a function of the momentum eigenvalue k , $4q = (kl)^2$. By simultaneously solving Eqs. (24) and (25) in the real space, we obtain the following form of the corresponding eigenfunctions (see App. D for details)

$$\Phi_{q,m}(r, \varphi) = \frac{1}{\sqrt{2\pi}} e^{im\varphi} \left(1 - \frac{r^2}{l^2}\right)^\lambda \left[A_m(k) r^m {}_2F_1\left(\lambda, \lambda+m; m+1; \frac{r^2}{l^2}\right) + B_m(k) r^{-m} {}_2F_1\left(\lambda, \lambda-m; 1-m; \frac{r^2}{l^2}\right) \right], \quad (45)$$

where ${}_2F_1(a, b; c; d)$ is the hypergeometric function and the parameter $\lambda = \frac{1}{2} + \frac{\sqrt{1-(kl)^2}}{2}$, with $(kl)^2 > 1$, and therefore $\lambda = \frac{1}{2} + is$, $s \in \mathbb{R}$. The coefficients $A_m(k)$ and $B_m(k)$ are normalization constants. Then the eigenvalue

of the Casimir operator can be expressed as $q = \lambda(1-\lambda) = \frac{1}{4} + s^2$, which corresponds to the principle series of irreducible representations, $q \geq \frac{1}{4}$ [63]. Here, quantum number m has a gap except for case when $q = \frac{1}{4}$. Notice that as the boundary is approached, $r \rightarrow l$, the wave-

function of the symmetry-adapted basis tends to zero.

We emphasize that a group of Möbius transformations acting on the disk \mathbb{D} is referred to as a discrete Fuchsian group if it acts discontinuously, i.e., any compact subset of \mathbb{D} intersects only finitely many of its images under the group [64]. In Sec. III, we utilize this structure to discretize the Poincaré disk, and in Sec. IV, we employ it to construct the corresponding discrete spin connection for the hyperbolic lattice.

C. Spinors on the Poincaré disk

In this section, we investigate the properties of spinors in the long-wavelength limit as a preliminary step toward the construction of the discrete spin connection and the embedding of spinor fields on a hyperbolic lattice. To this end, we introduce an *expanded Poincaré disk* geometry, where the addition of a temporal coordinate extends the Poincaré disk metric to the form

$$G(t, x, y) = \begin{pmatrix} -1 & 0 & 0 \\ 0 & \frac{1}{(1 - \frac{x^2 + y^2}{l^2})^2} & 0 \\ 0 & 0 & \frac{1}{(1 - \frac{x^2 + y^2}{l^2})^2} \end{pmatrix}. \quad (46)$$

Since the time coordinate is incorporated as a flat direction, this modification does not introduce additional nonzero Christoffel symbols in the geometry.

The dynamics of a massive fermion in this background are governed by the Dirac equation in natural coordinates, including the spin connection ω_μ^{ab} ,

$$\left[e^\mu_a \gamma^a \left(\partial_\mu + \frac{1}{2} \omega_\mu^{cb} \Sigma_{cb} \right) - m \right] \Psi(x) = 0, \quad (47)$$

where e^μ_a are the vielbeins, and the helicity operator is given by $\Sigma_{cb} = \frac{1}{4} [\gamma_b, \gamma_c]$. Here, Greek indices $\mu \in \{t, x, y\}$ label coordinates on the Poincaré disk, while Latin indices $a, b, c \in \{0, 1, 2\}$ denote the local (Minkowski) frame.

By solving the stationary Dirac equation (47), we obtain explicit spinor solutions on the hyperbolic disk, as detailed in Appendix D. These results are employed for the calculation of physical observables, such as the density of states via the corresponding Green's function, discussed in the subsequent section.

We now determine the symmetry generators of the Dirac field on the Poincaré disk. To this end, we focus on stationary solutions of the Dirac equation, restricting the Greek indices to spatial coordinates. These generators satisfy the algebraic structure defined by the Killing vectors, as given in Eqs. (13)–(15).

The infinitesimal coordinate transformation $x \rightarrow x' = x + \delta x$ takes the form

$$\delta x^\mu = w^\mu{}_\nu x^\nu + 2(c \cdot x) x^\mu - c^\mu (x^2 + l^2), \quad (48)$$

where $w^{\mu\nu} = \theta \varepsilon^{\mu\nu}$, with $\varepsilon^{\mu\nu}$ the Levi-Civita tensor. This, in turn, motivates to represent a general variation of the

spinor field's form under this transformation as follows:

$$\delta_0 \Psi(x) = \left(\frac{1}{2} w^{\mu\nu} M_{\mu\nu} + c^\mu K_\mu \right) \Psi(x), \quad (49)$$

where the generators read

$$M_{\mu\nu} = M_{\mu\nu}{}^\rho \partial_\rho + M_{\mu\nu}^{(0)}, \quad (50)$$

$$K_\mu = K_\mu{}^\rho \partial_\rho + K_\mu^{(0)}. \quad (51)$$

The explicit form of the spinor transformation is fixed by requiring invariance of the Dirac equation; see Appendix E for details. The resulting symmetry generators are

$$K_x = (-l^2 + x^2 - y^2) \partial_x + 2xy \partial_y + iy \sigma_z, \quad (52)$$

$$M = x \partial_y - y \partial_x + i \frac{\sigma_z}{2}, \quad (53)$$

$$K_y = 2xy \partial_x + (-l^2 - x^2 + y^2) \partial_y - ix \sigma_z, \quad (54)$$

where the coordinate parts correspond precisely to the Killing vectors in Eqs. (7)–(9).

The associated Casimir operator is given by

$$\Xi^2 = \xi^2 + \left(1 - \frac{x^2 + y^2}{l^2} \right) \frac{i \sigma_z}{2} M, \quad (55)$$

with M as in Eq. (53). The eigenvalue equation,

$$\Xi^2 \Psi(x) = \kappa \Psi(x), \quad (56)$$

yields eigenfunctions corresponding to solutions of the Dirac equation (see Appendix D), with

$$\kappa = \frac{1}{4} \left(E^2 - m^2 + \frac{1}{l^2} \right). \quad (57)$$

These symmetry generators form the basis for the analysis of spinor field transformations under discrete lattice symmetries.

D. Density of states

Here we calculate the density of states (DOS) of Dirac fermions in D -dimensional hyperbolic space with $2 \leq D \leq 4$, to show that the coupling to the spin connection introduces a finite density of states at zero energy. We find the DOS from the corresponding Green's function $G(x, y)$ in the real space

$$\left[e^\mu_a \gamma^a \left(\partial_\mu + \frac{1}{2} \omega_\mu^{cb} \Sigma_{cb} \right) - m \right] G(x, y) = i \delta(x - y), \quad (58)$$

with x and y as coordinates in the real space, C is a constant and $\delta(x)$ is the Dirac delta function. We also define an auxiliary function $S(x, y)$ as

$$\left[e^\mu_a \gamma^a \left(\partial_\mu + \frac{1}{2} \omega_\mu^{cb} \Sigma_{cb} \right) + m \right] S(x, y) = G(x, y), \quad (59)$$

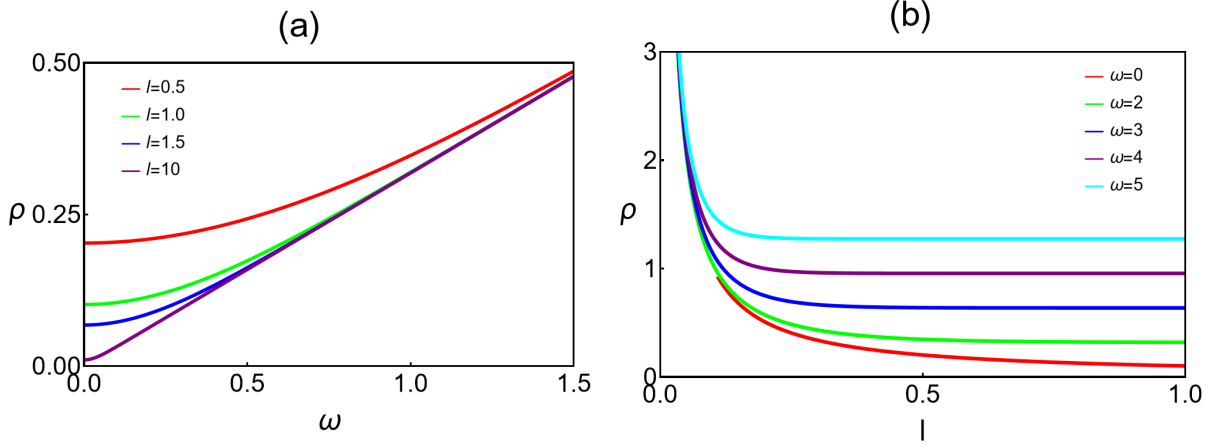


Figure 3. The density of states (DOS) for Dirac fermions in the two-dimensional hyperbolic space, as given by Eq. (63). (a) The DOS as a function of energy for several values of the radius of the hyperbolic space, l . We observe that $\rho(\omega = 0)$ tends to zero as l increases, while for any finite l , the zero-energy DOS, $\rho(\omega = 0)$, is finite. Notice that in the regime $\omega \gg l^{-1}$, the DOS approaches the linear scaling with energy, $\rho(\omega) \sim \omega$, consistent with the flat-space result. (b) The DOS as a function of the radius l , $\rho(l)$, for different energies. Notice that for $\omega \rightarrow 0$, the DOS is finite, for any finite radius, l (red curve), while for any non-zero energy, the DOS approaches a finite value as l increases.

which we substitute into Eq. (58). Given that the time coordinate is associated with energy for vanishing spin connection, we will treat energy as a parameter, allowing to define the parameter $s^2 = E^2 - m^2$, directly related to the (real) energy. An ansatz for the auxiliary func-

tion contains a matrix part $U(x, y)$ and a function of the distance between two different points in space, with the condition $U(x, x) = 1$. The Green's function in D -dimensional hyperbolic space then takes the form [65],

$$G(x, y; s) = -i \frac{l^{1-D}}{(4\pi)^{\frac{D}{2}}} \frac{\Gamma(\frac{D}{2} + isl) \Gamma(isl + 1)}{\Gamma(2isl + 1)} \left[\cosh\left(\frac{d}{2l}\right) \right]^{1-D-sl} \times \\ \left[U(x, y) \cosh\left(\frac{d}{2l}\right) {}_2F_1\left(\frac{D}{2} + isl, isl; 2isl + 1; \cosh^{-2}\left(\frac{d}{2l}\right)\right) + \right. \\ \left. + \gamma_i n^i U(x, y) \sinh\left(\frac{d}{2l}\right) {}_2F_1\left(\frac{D}{2} + isl, isl + 1; 2isl + 1; \cosh^{-2}\left(\frac{d}{2l}\right)\right) \right]. \quad (60)$$

The DOS in D -dimensional hyperbolic space is found from the Green's function as

$$\rho_D(\omega) = -\frac{1}{\pi} \lim_{\delta \rightarrow 0} \text{ImTr}\{G(x, y, s \rightarrow \omega + i\delta)\}, \quad (61)$$

where analytical continuation in energy is performed. It should be noted that, in the Matsubara (imaginary-time) formalism, the energy parameter is purely imaginary, taking the form $s \rightarrow is$, with $s \in \mathbb{R}$. To relate the Matsubara Green's function to physical observables defined for the real frequency, one performs analytic continuation by substituting $is \rightarrow \omega + i\delta$, where ω is the real frequency and $\delta > 0$ is infinitesimal.

We first focus on the calculation of the DOS in two-dimensional space, $D = 2$. After taking the trace of Eq.

(60), we find a divergence which we treat by employing the dimensional regularization, with $\varepsilon = 2 - D$. Taking the limit $\delta \rightarrow 0$ first, and then $D \rightarrow 2$ (equivalently, $\varepsilon \rightarrow 0$),

$$\rho_2(\omega, l) = -\frac{4}{\pi} \lim_{\varepsilon \rightarrow 0} \lim_{\delta \rightarrow 0} \text{Im} \frac{l^{\varepsilon-1}}{(4\pi)^{1-\frac{\varepsilon}{2}}} \times \frac{\Gamma(1 - \frac{\varepsilon}{2} - i\omega + \delta l) \Gamma(\frac{\varepsilon}{2})}{\Gamma(-i\omega + \delta l + \frac{\varepsilon}{2})}. \quad (62)$$

We then obtain

$$\rho_2(\omega, l) = -\frac{1}{\pi^2} \left(2\omega \text{Im}[\psi(-i\omega)] + \frac{1}{l} \right), \quad (63)$$

where $\psi(z)$ is the polygamma function, defined as $\psi(z) = d \ln \Gamma(z) / dz$. The plot of the DOS in the two-dimensional

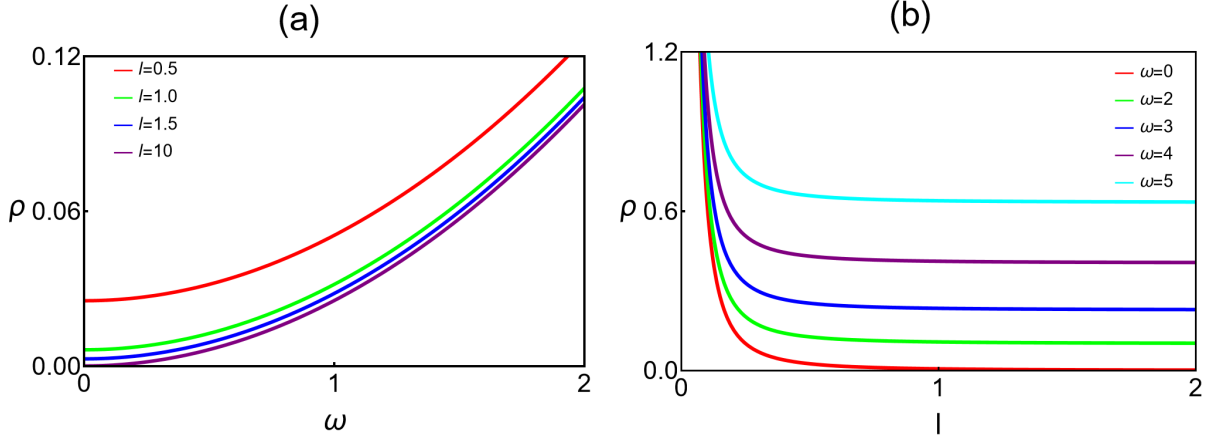


Figure 4. The density of states (DOS) for Dirac fermions in three-dimensional hyperbolic space, as given by Eq. (66). (a) The DOS as a function of energy for several values of the radius of the hyperbolic space, l . We observe that the zero-energy DOS is non-vanishing, but tends to zero as l increases. (b) The DOS as a function of the radius, l , for several values of the energy.

space is shown in Fig. 3. The flat space limit ($l \rightarrow \infty$) of the density of state function in two-dimensional space is given by

$$\rho_2(\omega, l \rightarrow \infty) = \frac{\omega}{\pi}, \quad (64)$$

which corresponds to the known form of the density of states for a four-component Dirac fermion in flat space with Fermi velocity set to unity. Importantly, in the zero-energy limit, $\omega \rightarrow 0$, the DOS is non-vanishing and it scales with the scalar curvature as $\rho(0, R) \sim |R|^{1/2}$, with the explicit form given by

$$\rho_2(0, R) = \frac{1}{\pi^2 \sqrt{8}} |R|^{1/2}, \quad (65)$$

and also in agreement with general scaling argument implying that the scaling dimension of the DOS [ρ] = $D - 1$, in units of momentum (inverse length), with the dynamic exponent $z = 1$, as it should be for a (pseudo-)relativistic system. Notice that this result agrees with the form obtained in Ref. [66] using a different approach.

For completeness, we also consider three-dimensional hyperbolic space, $D = 3$, yielding the DOS in the form

$$\rho_3(\omega, l) = \frac{\omega^2}{\pi^2} + \frac{1}{(2\pi l)^2}, \quad (66)$$

which therefore shows a separable form in the energy and the curvature. The effect of the curvature is to simply add a linear-in-curvature shift to the usual form of the DOS for 3D massless Dirac fermions in flat space, see also Figure 4. Remarkably, in the zero-energy limit $\omega \rightarrow 0$, the DOS is non-zero and linearly scales with the curvature,

$$\rho_3(\omega = 0, R) = \frac{|R|}{8(2\pi)^2}. \quad (67)$$

On the other hand, in the limit $l \rightarrow \infty$ ($R \rightarrow 0$), we recover the well known result in the flat space,

$$\rho_3(\omega, l \rightarrow \infty) = \frac{\omega^2}{\pi^2}. \quad (68)$$

Similarly, in $D = 4$, we find

$$\rho_4(\omega, l) = -\frac{\omega}{4\pi^3 l^2} (1 + l^2 \omega^2) \text{Im} [\psi(2 - il\omega) + \psi(-1 - il\omega)], \quad (69)$$

also featuring finite zero-energy DOS given by

$$\rho_4(\omega = 0, R) = \frac{|R|^{3/2}}{64\pi^3 \sqrt{2}}. \quad (70)$$

Furthermore, the flat-space limit of the DOS is

$$\rho_4(\omega, l \rightarrow \infty) = \frac{\omega^3}{4\pi^2}, \quad (71)$$

in agreement with the result obtained by calculating the DOS of Dirac fermions directly in $D = 4$ flat space.

III. Discretization of Poincaré disk

Motivated by this nontrivial behavior of the Dirac fermions coupled to the spin connection in the hyperbolic space, we now consider discretization of the Poincaré disk. To this end, in this Section we obtain the discrete symmetries of a hyperbolic lattice starting from their continuum counterparts on the Poincaré disk, and thus consider the point group symmetry of the unit cell, in Sec. III A, and the translations, in Sec. III B. For convenience, we place the center of a polygon at the origin of the tessellated Poincaré disk and systematically organize the polygons into successive generations, as illustrated in Fig. 5.

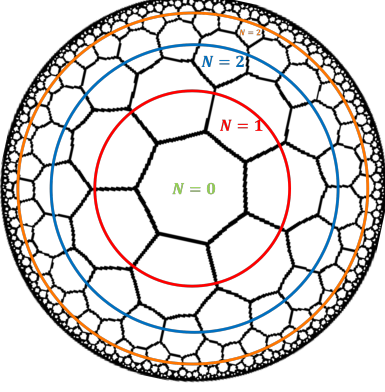


Figure 5. Schematic representation of the $\{7, 3\}$ hyperbolic lattice, illustrating the hierarchical organization of polygons by generation for a tessellation of the Poincaré disk with Schläfli symbol $\{p, q\}$. The central polygon, corresponding to $N = 0$, constitutes the zeroth generation. The red circle marks polygons belonging to the first generation ($N = 1$), the blue circle encloses those in the second generation ($N = 2$), and the orange circle marks the third generation ($N = 3$). Subsequent generations can be identified analogously.

A. Point group symmetry

We begin by constructing the cyclic point group corresponding to the Möbius transformation given in Eq. (17). This construction is then used to derive the explicit form of discrete rotational symmetries on the tessellated Poincaré disk.

To determine the structure of the point group operations, we recall that repeated application of a group element eventually yields the identity transformation; the number of applications required is referred to as the order of the element. Specifically, we consider the symmetry transformation corresponding to the application of the transformation p times to a given point, as follows:

$$z^{(1)} = e^{i\tilde{\theta}} \frac{z - c}{1 - \bar{c}z}, \quad (72)$$

$$z^{(2)} = e^{i\tilde{\theta}} \frac{z^{(1)} - c}{1 - \bar{c}z^{(1)}}, \quad (73)$$

$$\vdots, \quad (74)$$

$$z^{(p)} = e^{i\tilde{\theta}} \frac{z^{(p-1)} - c}{1 - \bar{c}z^{(p-1)}}. \quad (75)$$

We can thus identify parameters θ_p and c_p after every transformation as:

$$e^{i\theta_p} = e^{i\tilde{\theta}} \frac{e^{i\theta_{p-1}} + c\bar{c}_{p-1}}{1 + \bar{c}c_{p-1}e^{i\theta_{p-1}}}, \quad (76)$$

$$c_p = \frac{c_{p-1}e^{i\theta_{p-1}} + c}{e^{i\theta_{p-1}} + c\bar{c}_{p-1}}, \quad p \in \mathbb{N}. \quad (77)$$

Let us assume that after applying the transformation p times, we obtain $z^{(p)} = z$, that corresponds to the unit (trivial) element of the discrete group. This then yields the conditions on the parameters,

$$e^{i\theta_p} = 1, \quad c_p = 0, \quad (78)$$

which result in the constraints on the arbitrary parameters,

$$c_{p-k}e^{i\theta_{p-k}} = -c_k. \quad (79)$$

Finally, the condition imposed on the parameters of continuum group symmetry to yield the point group is given by:

$$1 + \cos \tilde{\theta} = (1 - |c|^2) \left(1 + \cos \frac{2n\pi}{p} \right), \quad (80)$$

where $n \in \{1, \dots, p-1\}$. We connect these parameters to those introduced in Eq. (16) for the continuous Möbius transformation, as follows:

$$\begin{aligned} \frac{1 + \cos \tilde{\theta}}{1 - |c|^2} &= 1 + \cosh(\sqrt{-\theta^2 + 4|a|^2}) \\ \Rightarrow \cosh(\sqrt{-\theta^2 + 4|a|^2}) &= \cos \frac{2n\pi}{p}, \quad \theta \geq 2|a| \\ \Rightarrow \sqrt{\theta^2 - 4|a|^2} &= \pm \frac{2n\pi}{p} + k\pi, \quad k \in \mathbb{Z}. \end{aligned} \quad (81)$$

In this way, we constructed the simplest discrete group for our problem, with just one generator of the order p , otherwise known as the cyclic group, C_p in the standard notation.

Next, we determine the rotations around an arbitrary point z_o of the tessellated Poincaré disk in which the center of a polygon is positioned at the center of the disk and employ polygon generations, as illustrated in Fig. 5. To this end, we first perform the transformation that brings an arbitrary point to the origin,

$$z'_o = e^{i\tilde{\theta}} \frac{z_o - c}{1 - \bar{c}z_o}, \quad (82)$$

such that $z'_o = 0$, which in turn implies the form of the parameters given by

$$z_o = c, \quad \tilde{\theta} = 2n\pi, \quad (83)$$

where $n \in \mathbb{Z}$. We then choose parameter $\tilde{\theta} = 0$, i.e. $n = 0$. The rotations are defined as

$$z'_R = e^{i\alpha} z', \quad (84)$$

where the primed coordinates denote the transformed coordinates of the site, while the inverse transformation reads

$$z_R = \frac{z'_R + z_o}{1 + \bar{z}_o z'_R}. \quad (85)$$

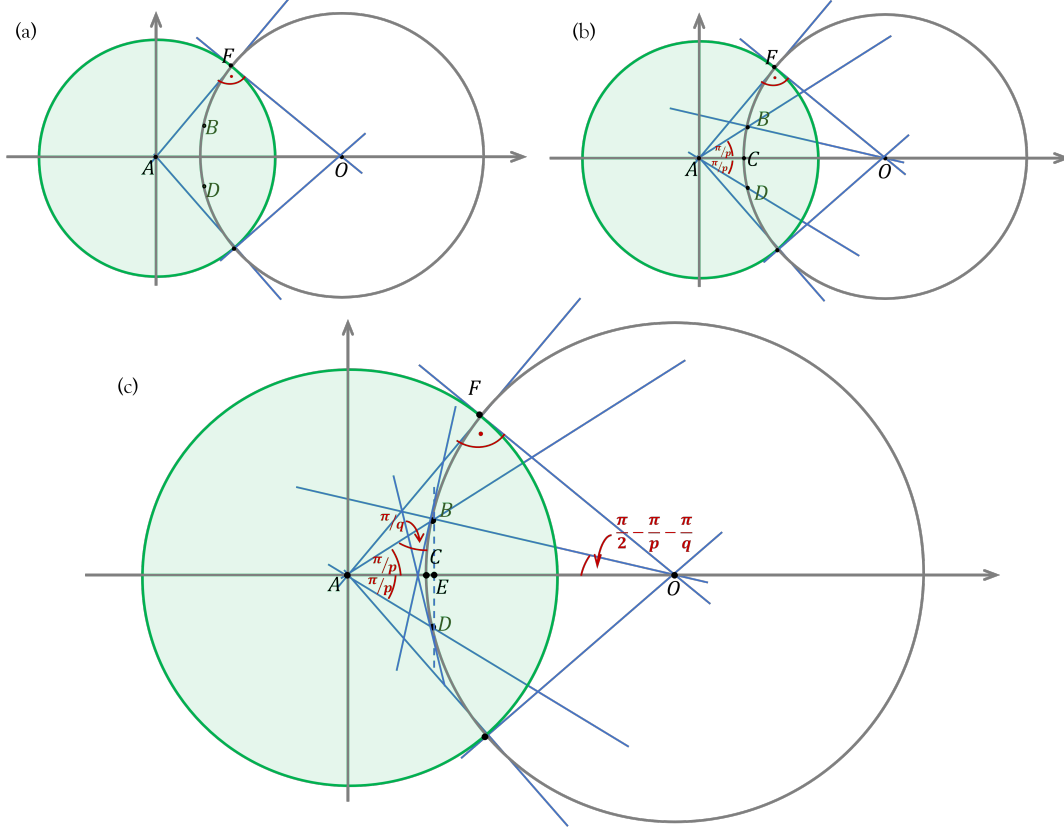


Figure 6. Geometric construction within the Poincaré disk, illustrating the main quantities for defining the hyperbolic p, q lattice. The disk is centered at point $A(0, 0)$, and its geodesic is represented as a circular arc of radius R centered at $O(\kappa + R, 0)$. (a) Geodesics in the Poincaré disk correspond to circles orthogonal to the disk boundary. At point F , a right triangle $\triangle AFO$ can be constructed. Points B and D indicate two vertices of a regular p -gon centered at A and lying on the same geodesic. (b) We denote the Euclidean distance from the center of the disk to the nearest points of the hyperbolic lattice r_0 , i.e. $AB = AD = r_0$. Point C marks the intersection of the x -axis, passing through A and O , with the geodesic circle, such that $AC = \kappa$. As we deal with regular p -gons on the $\{p, q\}$ hyperbolic lattice, an important angle in the construction is given as $\angle BAC = \angle CAD = \frac{\pi}{p}$. (c) Another important angle is $\angle ABD = \angle ADB = \frac{\pi}{q}$. The shortest Euclidean distance from point B (D) to the line AO is indicated by BE (DE), depicted as a dotted line.

Finally, the discrete rotations on the lattice embedded in the Poincaré disk take the form

$$z_R = \frac{e^{i\alpha} - |z_o|^2}{1 - |z_o|^2 e^{i\alpha}} \frac{z - z_o \frac{e^{i\alpha} - 1}{e^{i\alpha} - |z_o|^2}}{1 - \bar{z}_o \frac{1 - e^{i\alpha}}{1 - |z_o|^2 e^{i\alpha}} z}, \quad (86)$$

where the parameters of the rotation, as defined in Eq. (17), are given by

$$c = z_o \frac{e^{i\alpha} - 1}{e^{i\alpha} - |z_o|^2}, \quad (87)$$

$$e^{i\tilde{\theta}} = \frac{e^{i\alpha} - |z_o|^2}{1 - |z_o|^2 e^{i\alpha}}. \quad (88)$$

The choice of Schläfli symbols, which characterize the tessellation of the Poincaré disk, therefore uniquely determines the rotation parameter α and, consequently, fully specifies the discrete rotational symmetries of the lattice.

B. Translations

In the previous subsection, we derived the conditions under which the continuum symmetry of space reduces to the discrete symmetry of a lattice, as captured by Eq. (80). We now turn to the construction of discrete transformations corresponding to translations inherited from flat space.

To proceed, we first determine the distance from the center of the Poincaré disk to the nearest site of the $\{p, q\}$ hyperbolic lattice. This calculation purely flat-geometrically by tracing the appropriate geodesic curves. As illustrated in Fig. 6, when the origin coincides with the disk center, these geodesics appear as circles orthogonal to the boundary of the disk, a property that will play a crucial role in our analysis.

We introduce the following notation for the relevant distances, as depicted in Fig. 6,

$$AC = \kappa, \quad OC = OF = OB = R, \quad (89)$$

$$AB = AD = r_0, \quad (90)$$

which satisfy the relations

$$(\kappa + R)^2 = 1 + R^2, \quad (91)$$

$$r_0 \sin \frac{\pi}{p} = R \sin \left(\frac{\pi}{2} - \frac{\pi}{p} - \frac{\pi}{q} \right), \quad (92)$$

$$\kappa + R = r_0 \cos \frac{\pi}{p} + R \cos \left(\frac{\pi}{2} - \frac{\pi}{p} - \frac{\pi}{q} \right). \quad (93)$$

Here, Eq. (91) is the Pythagorean relation for the triangle $\triangle AFO$, Eq. (92) gives the shortest distance from B to the line AO , and Eq. (93) specifies the distance between A and O .

Solving these equations yields the exact distance from the center to the nearest site, which depends only on the Schläfli symbols:

$$r_0 = \sqrt{\frac{\cos \left(\frac{\pi}{p} + \frac{\pi}{q} \right)}{\cos \left(\frac{\pi}{p} - \frac{\pi}{q} \right)}}. \quad (94)$$

Similarly, we obtain the distance from the center A to the nearest circular geodesic at point C as

$$\kappa = \frac{\cos \frac{\pi}{q} - \sin \frac{\pi}{p}}{\sqrt{\cos \left(\frac{\pi}{p} + \frac{\pi}{q} \right) \cos \left(\frac{\pi}{p} - \frac{\pi}{q} \right)}}. \quad (95)$$

Since we are after the form of translations, we now compute the corresponding hyperbolic distance,

$$d_\kappa = \frac{1}{2} \operatorname{arcosh} \left(\frac{\cos \frac{\pi}{q}}{\sin \frac{\pi}{p}} \right). \quad (96)$$

with the hyperbolic distance between two polygon centers being $2d_\kappa$. Furthermore, the Euclidean distance d_E between these centers, obtained from Eq. (22), is given by

$$d_E = \sqrt{1 - \frac{\sin^2 \frac{\pi}{p}}{\cos^2 \frac{\pi}{q}}}. \quad (97)$$

To construct discrete translation transformations analogous to those in flat space, we then consider a translation from the origin $z = 0$ to two nearest rings of polygons. Generalizing to an arbitrary point z , the transformation takes the form

$$z' = t_m z = \frac{z + d_E e^{i \frac{2\pi m}{p}}}{1 + d_E z e^{-i \frac{2\pi m}{p}}}, \quad (98)$$

where $m \in \{0, \dots, p-1\}$. This allows to write the normalized translation operator t_m in matrix representation as

$$t_m = \frac{1}{1 - d_E^2} \begin{pmatrix} 1 & d_E e^{i \frac{2\pi m}{p}} \\ d_E e^{-i \frac{2\pi m}{p}} & 1 \end{pmatrix}. \quad (99)$$

If we now proceed along a fixed direction (given by m), to reach the N -th generation of polygons, the transformation must be applied N times, yielding

$$t_m^n = \frac{1}{2(1 - d_E^2)^n} \begin{pmatrix} (1 + d_E)^n + (1 - d_E)^n & e^{i \frac{2\pi m}{p}} [(1 + d_E)^n - (1 - d_E)^n] \\ e^{-i \frac{2\pi m}{p}} [(1 + d_E)^n - (1 - d_E)^n] & (1 + d_E)^n + (1 - d_E)^n \end{pmatrix}. \quad (100)$$

Finally, to relate these results to the Lie group parameters of the Poincaré disk, as introduced in Eq. (16), the translation parameters take the form,

$$a = -\operatorname{arctanh} d_E e^{i \frac{2\pi m}{p}}, \quad (101)$$

$$\bar{a} = -\operatorname{arctanh} d_E e^{-i \frac{2\pi m}{p}}, \quad (102)$$

$$\tilde{\theta} = 0, \quad (103)$$

which will be used in the next section to construction the discrete spin connection.

IV. Construction of the discrete spin connection

In this section, we formulate the action for Dirac fermions on a hyperbolic lattice, explicitly incorporating the effects of spin-curvature coupling. The central object in this construction is the *discrete spin connection*, which plays the role of the lattice analogue of its continuum counterpart. Following the approach in Ref. [60], we begin by considering a simplicial Riemannian manifold and, through the implementation of parallel transport on the hyperbolic lattice, derive the explicit form of the discrete spin connection.

Let us first introduce the notation used for the simplicial manifold. Sites will be denoted by i, j, k , assigned lengths from Regge calculus will be l_{ij} and link volumes with V_{ij} :

$$l_{ij} = |\sigma_1(ij)|, \quad V_{ij} = |\sigma_1(ij) \wedge \sigma_1^*(ij)|, \quad (104)$$

where $\sigma_1(ij)$ is 1-dimensional simplex and σ_1^* is its dual. The action for the lattice Dirac fermions can be written as

$$S = \frac{1}{2} \sum_{\langle i,j \rangle} \frac{V_{ij}}{l_{ij}} \left[\bar{\psi}_i e_a^{(i)j} \gamma^a \Omega_{ij} \psi_j - \bar{\psi}_j \Omega_{ji} e_a^{(i)j} \gamma^a \psi_i \right] + \frac{1}{2} m V_i \bar{\psi}_i \psi_i + S_{\text{WilsonTerm}}, \quad (105)$$

where $V_i = |\sigma_0^*(i)|$ is normalized dual volume and Ω_{ij} is the connection matrix, i.e. the discrete spin connection. We emphasize that the connection matrix plays a similar role as the compact Wilson gauge variables $U_\mu = e^{iA_\mu(x)}$, for instance, those for color spinors in lattice gauge theories [67]. To avoid the doubler states, coming from naively using the finite element method, we add the Wilson term,

$$S_{\text{WilsonTerm}} = \frac{1}{2} \sum_{\langle i,j \rangle} \frac{V_{ij}}{l_{ij}^2} (\bar{\psi}_i - \bar{\psi}_j \Omega_{ji}) (\psi_i - \Omega_{ij} \psi_j), \quad (106)$$

which is equivalent to the lattice Laplace-Beltrami operator for scalar fields in arbitrary gauge. Furthermore, this discrete connection should follow the lattice realization of tetrad hypothesis,

$$e_a^{(j)i} \gamma^a = -\Omega_{ji} e_a^{(i)j} \gamma^a \Omega_{ij}, \quad (107)$$

which is gauge covariant under local $SU(1,1)$ transformations. Our goal is to write the action for fermions on sites that are nearest to the center of the disk, as we can obtain any other polygon by the transformation found in Sec. III.

To explicitly construct the connection matrix Ω_{ij} on the Poincaré disk, we begin by considering the form of the geodesics given in Eq. 21 and two lattice points on the $\{p, q\}$ hyperbolic lattice, as illustrated in Fig. 7. There are two possible approaches: one involves directly solving the parallel transport equation, while the other is based purely on geometric considerations, as detailed below. Next, we compute the corresponding Lorentz rotation O_{ij}^{ab} in $O(2)$. Each Lorentz rotation in $O(2)$ is then mapped to an element in $\text{Spin}(2)$, such that $O_{ij} \rightarrow s_{ij} \Omega_{ij}$, where the sign s_{ij} is chosen appropriately. This procedure yields the following explicit form for the connection matrix:

$$\Omega_{ij} = s_{ij} e^{i \frac{\sigma_z}{2} \theta_{ij}}, \quad (108)$$

where θ_{ij} is the difference between the angles of the tangent vectors at points i and j , that is, $\theta_{ij} = \alpha_i - \beta_j$, as depicted in Fig. 7.

Here, we present a purely geometric approach to determine the angle θ_{ij} required for constructing the discrete spin connection matrix which invokes explicit construction of tangent vectors of the relevant geodesic curves. For comparison, an alternative derivation based on directly solving the parallel transport equation is provided in App. F. The tangent vector for the geodesic curve given by Eq. (20) can be readily obtained, whereas for the orthogonal-circle geodesic described by Eq. (21), the tangent vector at each site takes the form

$$\mathbf{V}_{\gamma_i} = \cos \gamma_i \mathbf{e}_x + \sin \gamma_i \mathbf{e}_y, \quad (109)$$

where γ_i is given by

$$\gamma_i = \arctan \left(-\frac{x_c - x_i}{y_c - y_i} \right). \quad (110)$$

Here, (x_c, y_c) denote the coordinates of the center of the orthogonal circle, and (x_i, y_i) correspond to the position of the site at which the angle is evaluated. We note that the tangent vector in Eq. (109) is normalized with respect to the flat space metric.

To track the rotation of a vector as it moves between points, we introduce an additional flat-space reference vector V_{r_i} at each site, against which angle differences are measured. The angles α_i and β_j can then be determined from the scalar product,

$$\cos \angle(\mathbf{V}_i, \mathbf{V}_{r_i}) = \frac{\mathbf{V}_i \cdot \mathbf{V}_{r_i}}{|\mathbf{V}_i| |\mathbf{V}_{r_i}|}, \quad (111)$$

where \mathbf{V}_i represents the tangent vector \mathbf{V}_{γ_i} to the geodesic at the given site (or the parallel transported vector in the alternative procedure discussed in App. F). We further note that, when working with tangent vectors,

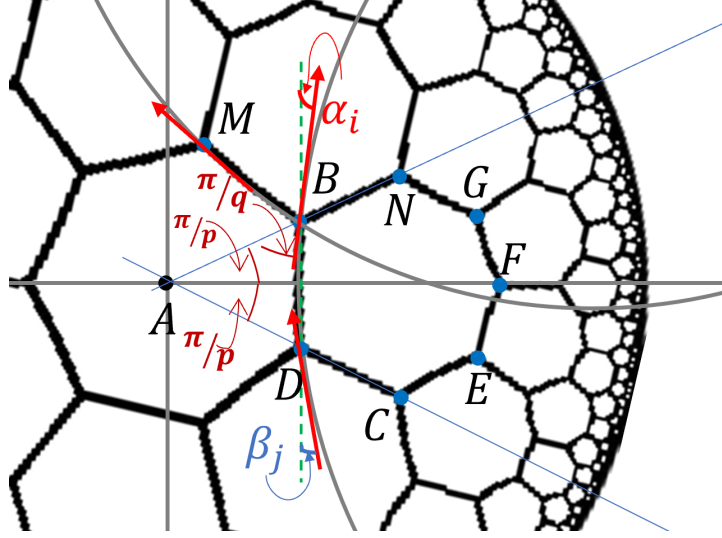


Figure 7. Illustration of tangent vectors (the red arrows) along geodesic paths in the $\{7,3\}$ hyperbolic lattice. The spinor undergoes a transformation, accompanying the corresponding phase shift, as it is transported from point $D(r_0 \cos \frac{\pi}{p}, -r_0 \sin \frac{\pi}{p})$ to point $B(r_0 \cos \frac{\pi}{p}, r_0 \sin \frac{\pi}{p})$ along one geodesic, and subsequently from B to $M(r_0 \cos \frac{3\pi}{p}, r_0 \sin \frac{3\pi}{p})$ along an adjacent geodesic. The figure depicts the $\{7,3\}$ tessellation of the Poincaré disk, with geometric parameters indicated for clarity. While illustrated for the $\{7,3\}$ case, this construction is applicable to general $\{p,q\}$ hyperbolic lattices.

the distinction between α_i and β_j introduced in Ref. [60] becomes unnecessary, as these angles can be identified within this framework, i.e., $\beta_j \rightarrow \alpha_j$.

To calculate the discrete spin connection throughout the Poincaré disk, it is important to find the coordinates of every site on the lattice. To this end, we start from the central polygon, where we find the coordinates of each site up to the angle in Eq. (94). Then we move on to the next generations of polygons utilizing that the tessellation of the Poincaré disk is regular and each polygon of the next generation shares two or more sites with the polygon from the previous generation, see Fig. 5.

A. Discrete spin connection in the zeroth generation polygons

For symmetry reasons, which can be easily checked, we can find the angle difference, θ_{ij} , between any two nearest points of the central polygon. We choose the orientation of the tessellation as depicted in Fig. 7 and select two points $D(r_0, -\frac{\pi}{p})$ and $B(r_0, \frac{\pi}{p})$.

Tangent vectors at point $D(r_0, -\frac{\pi}{p})$ and at point $B(r_0, \frac{\pi}{p})$ on the geodesic curve centered at point O , as shown in Fig. 7, can be found in the form given in Eq. (109), with the corresponding angles γ_D and γ_B of the form

$$\gamma_D = \arctan \frac{\kappa + R - r_0 \cos \frac{\pi}{p}}{r_0 \sin \frac{\pi}{p}}, \quad (112)$$

$$\gamma_B = \arctan \frac{r_0 \cos \frac{\pi}{p} - (\kappa + R)}{r_0 \sin \frac{\pi}{p}}, \quad (113)$$

with the parameters κ , r_0 and R given by Eqs. (89) and (90) for the central polygon. Reference vector [Eq. (111)] is chosen as

$$\mathbf{V}_{r_i} = \frac{a}{1 - r_0^2} \mathbf{e}_y. \quad (114)$$

Now, using Eq. (111), we can find the angle θ_{ij} determining the discrete spin connection on the central polygon in the form

$$\theta_{ij} = \pi - 2 \left(\frac{\pi}{p} + \frac{\pi}{q} \right) \quad (115)$$

Notice that the angle θ_{ij} in the spin connection, as well as r_0 , κ , and R , are determined solely by the Schläfli symbols $\{p, q\}$.

The next step is to construct the discrete spin connection matrix Ω_{ij} [Eq. (108)] for the central polygon, with details shown in App. F. The sign ambiguity for the discrete spinor matrix connection here is given by $s_{ij} = (-1)^{pq}$. As can be directly checked, the derived connection matrix Ω_{ij} satisfies the global constraint that integrated curvature on every polygon in the continuum limit vanishes, with the gauge condition given as

$$(\Omega_{12}\Omega_{23}\dots\Omega_{p-1p})^{1/p} \approx 1, \quad (116)$$

which is the condition for approaching the Dirac equation in the continuum limit.

B. Discrete spin connection on the polygons in farther generations

Given the regularity of the disk tessellation, the explicit forms of discrete rotations and translations derived

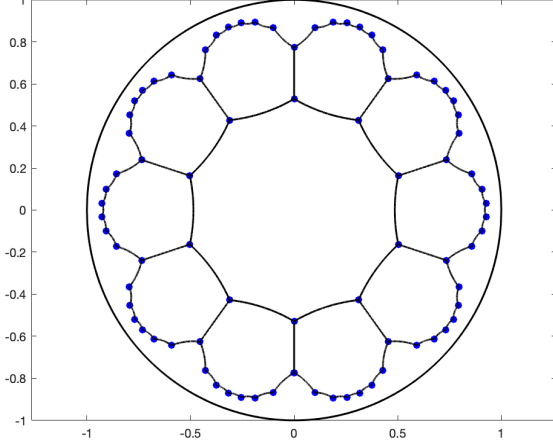


Figure 8. Illustration of the $\{10,3\}$ tessellation of the Poincaré disk. Each vertex corresponds to a lattice site, with edges connecting nearest neighbors forming regular decagons. The values of the coordinates of the sites are given in Table I. The blue dots indicate the positions of the sites comprising the first two generations in the hyperbolic lattice.

in Sections III A and III B can be systematically employed to determine the coordinates of all sites in each subsequent generation of polygons. To this end, as a first step, we identify the centers of each new polygon by applying the translation matrix introduced in Eq.(100). We denote the center of the polygon under consideration as z_o , which serves as the reference point for subsequent rotational operations. We then select one of the coordinates z that is shared with the previous generation and perform a rotation by an angle $\frac{2\pi}{p}$ about z_o , utilizing Eq.(86) to carry this out.

Once we find the coordinates (x_i, y_i) of each site, we can obtain the geodesic curve corresponding to those sites using Eqs. (20) and (21). One should be careful, however, with the choice of the geodesics that connect two points. If the appropriate geodesics curve is given as Eq. (21), we obtain the center of geodesic (x_c, y_c) . Now, with the parallel transported vectors derived in Eqs. (F15) and (F16), we can find angles α_i and β_j from the scalar product, which in turn yields the angle θ_{ij} between every

nearest two points.

Let us now focus on the first generation of polygons, corresponding to $N = 1$ in Fig. 5. By following the procedure outlined above, the centers of the polygons in this generation are given by

$$z_o = d_E e^{i \frac{2\pi m}{p}}, \quad m \in 1, 2, \dots, p. \quad (117)$$

The construction of the discrete spin connection for the sites of a single polygon in the first generation can be readily generalized to all polygons within the same generation. For definiteness, we proceed by considering the case $m = 0$. In this setting, the two sites shared between the central polygon and the selected first-generation polygon are denoted as $B(r_0, \frac{\pi}{p})$ and $D(r_0, -\frac{\pi}{p})$, as shown in Fig. 7. Either of these sites may serve as the initial point for the application of the discrete rotation transformation given by Eq. (86). By successively rotating by steps of $2\pi/p$, one obtains the full set of sites constituting the polygon of interest.

The sites B and N , as well as D and C (see Fig. 7), are connected by geodesic curves of the type given by Eq.(20). For these pairs, the vectors V_{γ_i} , tangent to the geodesic curves, can be expressed in terms of their slopes as

$$\mathbf{V}_{\gamma_{\pm}} = \cos \frac{\pi}{p} \mathbf{e}_x \pm \sin \frac{\pi}{p} \mathbf{e}_y. \quad (118)$$

Since, in this case, the geodesic is a straight line, a tangent vector from N to B or from D to C remains invariant. For all other pairs of sites, the connection is realized by a geodesic curve of the form given by Eq. (21), for which the coordinates of the corresponding geodesic center (x_c, y_c) should be determined.

To illustrate the aforementioned construction, we consider the $\{10,3\}$ tessellation of the Poincaré disk (see Fig. 8) and explicitly determine the discrete spin connection for the first generation of polygons. The resulting values of the relative angles, determining the spin connection as given by Eq. (108), for a representative polygon in the first generation are presented in Table I. The accompanying Matlab code, utilized for these computations, systematically generates the relevant parameters for all polygons in the first generation and is applicable to an arbitrary $\{p,q\}$ tessellation of the Poincaré disk. In addition, we confirm that the lattice realization of the tetrad hypothesis, Eq.(107), is satisfied [68].

Using the previously obtained form of the discrete spin connection, the action for the nearest-neighborhood interaction reads

$$S = \frac{1}{2} \sum_{m,n}^p \sum'_{i_1, i_2, \dots, i_p} \sum'_{j_1, j_2, \dots, j_p} \frac{V_{mn}}{l_{mn}} \left[\bar{\psi}(t_{i_1}^{j_1} t_{i_2}^{j_2} \dots t_{i_p}^{j_p} x) e_a \gamma^a \Omega(\theta_{ij}) \psi(t_{i_1}^{j_1} t_{i_2}^{j_2} \dots t_{i_p}^{j_p} x) \delta_{m,n+1} + \dots \right], \quad (119)$$

where the first sum is for the central polygon, the second sum is counting transformations and the third sum is

z_i	Site coordinates	Radius of the geodesic $R_i(z_i, z_{i+1})$	$\theta_{i,i+1}$
z_1	{0.503048,-0.16345}	∞	0
z_2	{0.735364,-0.238934}	0.300283	-0.4685
z_3	{0.857778,-0.172252}	0.134291	-0.6790
z_4	{0.857778,-0.172252}	0.0927926	-0.7633
z_5	{0.926772,-0.0317908}	0.0829962	-0.7862
z_6	{0.926772,0.0317908}	0.0927926	-0.7633
z_7	{0.908171,0.0983609}	0.134291	-0.6790
z_8	{0.857778,0.172252}	0.300283	-0.4685
z_9	{0.735364,0.238934}	∞	0
z_{10}	{0.503048,0.16345}	0.786151	0.4189

Table I. Parameters characterizing a representative polygon in the first generation, taken to be mirror-symmetric about the x -axis, see Fig. 8. The first column lists the coordinates of each site of the selected polygon. The second column provides the radius of the geodesic connecting each pair of consecutive sites; a value of ∞ indicates a geodesic of type Eq. (20). The listed radii are identical for all polygons in the first generation. The third column displays the angle $\theta_{i,i+1}$, which is required for the computation of the connection matrix $\Omega_{i,i+1}$ entering the discrete spin connection, given by Eq. (108). For $i = 10$, $\theta_{i,i+1}$ corresponds to the angle between the tenth and first sites of the polygon. This angle is shared with the zeroth generation and therefore coincides with the corresponding angle defined in Eq. (115). Notice that θ_{ij} are equal for the bonds i, j related by the mirror reflection about the x -axis (Fig. 8).

counting the number of generations from the center of the Poincaré disk to the edge placed at the infinity of the disk. Note that these sums should not include the overlapping cells that can be reached differently which is denoted by \sum' .

V. Conclusions and outlook

In this work, we have systematically incorporated spin-curvature coupling into the study of fermions on hyperbolic lattices by utilizing the isometries of the Poincaré disk model. Constructing spinors from the irreducible representations of the projective $SU(1,1)$ group, we established a direct connection between Dirac fermions and their coupling to the spin connection of hyperbolic space. As a result, the DOS at zero energy is finite, following the scaling relation $\rho(0) \sim |R|^{(D-1)/2}$ for spatial dimensions $2 \leq D \leq 4$. This result elucidates the fundamental influence of curvature on the electronic properties of the system. To establish a precise correspondence with discrete hyperbolic lattices, we have determined the explicit forms of their discrete translational and rotational symmetries, which are uniquely specified by the Schläfli symbols $\{p, q\}$.

As a next step, building on these symmetries and employing approach in Ref. [60], we constructed a discrete spin connection that depends solely on the lattice geometry, paving the way for a deeper understanding of the behavior of Dirac fermions in hyperbolic space. Since for hyperbolic tilings with $p \pmod{4} = 2$ for $p > 6$, and $q = 3$, the system hosts linearly dispersing Dirac fermions in the absence of the coupling to spin connection [42], these structures thus offer an ideal platform to test our theoretical predictions and further unravel the rich physics of hyperbolic materials. For instance, our results should motivate numerical studies of the lattice models of interacting Dirac fermions incorporating the discrete spin connection in quantum Monte Carlo simulations, as has been carried out for short-range inter-

acting Dirac fermions in flat space [69–71]. Our findings should further motivate to reconsider the corresponding field-theoretical description of such phase transitions of Dirac fermions in terms of Gross-Neveu-Yukawa quantum-critical theories in the curved space [59].

It is important to emphasize that the spin-curvature coupling introduced here for lattice models of Dirac fermions opens new avenues for the exploration of topological states in curved geometries. A particularly compelling direction for future work is the investigation of curvature-induced topological phase transitions—specifically, whether the spin-curvature coupling proposed in this study can give rise to emergent topological phases, analogous to the role played by spin-orbit coupling in conventional quantum materials [72, 73]. An additional set of challenges lies in characterizing the appropriate topological invariants in this context, such as determining the precise form of the Chern number in the presence of a spin connection, and analyzing the resultant topological phase transitions. We note that initial progress in this direction has recently been made for spinless quasiparticles on hyperbolic space [38]; extending such analyses to systems with spin-curvature coupling represents an interesting open problem.

Our approach can be straightforwardly extended to the Poincaré ring representing a continuum embedding of time-constant slices of Bañados-Teitelboim-Zaneli (BTZ) black hole in $(2+1)D$ AdS space [74], which should reveal tessellations in this space and open the frontier studying the band structures therein. This may ultimately yield new insights into the effects of a black hole on the fermionic matter. In particular, such studies may also motivate simulations of BTZ black hole coupled to the

fermions, and exploration of the effects of ensuing topological bands, interaction effects, etc.

Finally, we point out that the experimental realization of our theoretical proposal appears to be well within reach, given recent advances in the engineering of spinless tight-binding models on hyperbolic lattices. Notably, such models have been successfully implemented in both topoelectric circuits [22] and optical lattice platforms [23, 36]. These experimental systems are capable of reproducing the essential features of the hyperbolic lattice geometry required by our construction. A key element in our analysis is the discrete spin connection, which, in the lattice context, manifests as a tunable phase factor associated with the hopping amplitudes. Such phase factors can already be routinely implemented in both topoelectric and optical lattice architectures, where local control over couplings and phases can be achieved with high precision through established experimental protocols.

Data availability

The data and software code for generating the figures presented in the main text and supplementary materials are available at [68].

Acknowledgments

We would like to thank Stefan Djordjević, Ilija Burić and Bitan Roy for fruitful discussions and useful comments. A.Dj. and M.D.Ć acknowledge the funding provided by the Faculty of Physics, University of Belgrade, through the grant number 451-03-136/2025-03/200162 by the Ministry of Science, Technological Development and Innovations of the Republic of Serbia. A.Dj. acknowledges the support by the Science Fund of the Republic of Serbia, grant number TF C1389-YF, Towards a Holographic Description of Noncommutative Space-time: Insights from ChernSimons Gravity, Black Holes and Quantum Information Theory - HINT. V. J. acknowledges the support by the Swedish Research Council Grant No. VR 2019-04735 and Fondecyt (Chile) Grant No. 1230933.

Appendix

A. Coordinate transformation and geodesics

In this section, we will explicitly derive Killing vectors, coordinate transformations and also give explicit calculation of equation of motion for a free particle.

To find an explicit form of Eq. (2) for the Killing vec-

tors, we first obtain the Christoffel symbols

$$\Gamma_{xx}^y = -\frac{1}{l^2} \frac{2y}{1 - \frac{x^2+y^2}{l^2}}, \quad (\text{A1})$$

$$\Gamma_{yy}^x = -\frac{1}{l^2} \frac{2x}{1 - \frac{x^2+y^2}{l^2}}, \quad (\text{A2})$$

$$\Gamma_{xy}^y = \frac{1}{l^2} \frac{2x}{1 - \frac{x^2+y^2}{l^2}}, \quad (\text{A3})$$

$$\Gamma_{yx}^x = \frac{1}{l^2} \frac{2y}{1 - \frac{x^2+y^2}{l^2}}. \quad (\text{A4})$$

Eq. (2) then explicitly reads as

$$\partial_x \xi_x = \frac{1}{l^2} \frac{2x}{1 - \frac{x^2+y^2}{l^2}} \xi_x - \frac{1}{l^2} \frac{2y}{1 - \frac{x^2+y^2}{l^2}} \xi_y, \quad (\text{A5})$$

$$\partial_y \xi_y = -\frac{1}{l^2} \frac{2x}{1 - \frac{x^2+y^2}{l^2}} \xi_x + \frac{1}{l^2} \frac{2y}{1 - \frac{x^2+y^2}{l^2}} \xi_y, \quad (\text{A6})$$

$$\partial_x \xi_y + \partial_y \xi_x = \frac{1}{l^2} \frac{4y}{1 - \frac{x^2+y^2}{l^2}} \xi_x + \frac{1}{l^2} \frac{4y}{1 - \frac{x^2+y^2}{l^2}} \xi_y. \quad (\text{A7})$$

By rising the indices of the components of Killing vector and summing Eq. (A5) and Eq. (A6) we arrive at the Cauchy-Riemann conditions (Eqs. (3) and (4)). Conformal Killing equation in two dimensions also turns to Cauchy-Riemann conditions, so further steps are analogous to that of solving conformal Killing equation. As mentioned in the main text, we can write symmetry transformations as a form of the analytic (Eq. (5)) and anti-analytic function (Eq. (6)). When applying this ansatz in Eq. (A5), we get conditions on parameters as

$$a_0 + \bar{a}_0 = 0, \quad (\text{A8})$$

$$a_1 + \bar{a}_{-1} = 0. \quad (\text{A9})$$

We conclude that the parameter a_0 is purely imaginary and can be written as $a_0 = i\theta$, $\theta \in \mathbb{R}$. Furthermore, we write parameter $a_{-1} = -a$, so parameter a_1 becomes $a_1 = \bar{a}$. These parameters will be used when finding the coordinate transformation generated by the Killing vectors. It is straightforward to derive vectors given by Eqs. (7), (8) and (9).

We now proceed to determine the coordinate transformations. We consider the transformation of $z = x + iy$ coordinate on the disk, as for $\bar{z} = x - iy$ coordinate can be done similarly. Starting from the algebra of Killing vectors, we construct the group element by exponentiation, as given by Eq. (16). Since the exponential function is analytical, we can expand the expression as a Taylor series to obtain,

$$z' = \frac{z_2 - z_1 e^{\sqrt{-\theta^2 + 4|a|^2}}}{z_2 e^{\sqrt{-\theta^2 + 4|a|^2}} - z_1} - z_1 z_2 \frac{1 - e^{\sqrt{-\theta^2 + 4|a|^2}}}{z_2 e^{\sqrt{-\theta^2 + 4|a|^2}} - z_1}, \quad (\text{A10})$$

$$z' = \frac{z \frac{1 - e^{\sqrt{-\theta^2 + 4|a|^2}}}{z_2 e^{\sqrt{-\theta^2 + 4|a|^2}} - z_1} + 1}{z_2 e^{\sqrt{-\theta^2 + 4|a|^2}} - z_1} + 1$$

where z_1 and z_2 read

$$z_1 = \frac{-\theta - \sqrt{-\theta^2 + 4|a|^2}}{2\bar{a}}, \quad (\text{A11})$$

$$z_2 = \frac{-\theta + \sqrt{-\theta^2 + 4|a|^2}}{2\bar{a}}. \quad (\text{A12})$$

To obtain the Möbius transformation (Eq. (17)) as the isometry of the Poincaré disk, we will redefine our parameters as

$$e^{i\theta} = \frac{z_2 - z_1 e^{\sqrt{-\theta^2 + 4|a|^2}}}{z_2 e^{\sqrt{-\theta^2 + 4|a|^2}} - z_1}, \quad (\text{A13})$$

$$c = z_1 z_2 \frac{1 - e^{\sqrt{-\theta^2 + 4|a|^2}}}{z_2 - z_1 e^{\sqrt{-\theta^2 + 4|a|^2}}}. \quad (\text{A14})$$

Let us now find the geodesic equation from conserved quantities together with the corresponding Killing vectors (Eq. (19)). Accordingly, we assign the constant C from Eq. (19) three distinct values, denoted C_1 , C_2 , and C_3 , each corresponding to the equations associated with the Killing vectors ξ_1 , ξ_2 , and ξ_3 , respectively. The explicit forms of the conserved quantities and the equations for the Killing vectors are given by

$$C_1 = \frac{1}{(1 - x^2 - y^2)^2} \left[\left(\frac{dx}{d\tau} \right)^2 + \left(\frac{dy}{d\tau} \right)^2 \right] \quad (\text{A15})$$

$$C_2 = \frac{dx}{d\tau} \frac{1}{(1 - x^2 - y^2)^2} \left(-y + x \frac{dy}{dx} \right) \quad (\text{A16})$$

$$C_3 = \frac{dx}{d\tau} \frac{1}{(1 - x^2 - y^2)^2} \left(2xy + \frac{dy}{dx} (-1 - x^2 + y^2) \right) \quad (\text{A17})$$

$$C_4 = \left(\frac{dx}{d\tau} \right)^2 \frac{1}{(1 - x^2 - y^2)^2} \left(1 + \left(\frac{dy}{dx} \right)^2 \right). \quad (\text{A18})$$

We introduce another constant $D_1^2 = \frac{C_4}{C_2^2}$ to get a solvable form,

$$x \frac{dy}{dx} - y = \frac{1}{D_1} (1 - x^2 - y^2) \sqrt{1 + \left(\frac{dy}{dx} \right)^2}. \quad (\text{A19})$$

Using this in the geodesic equation,

$$\frac{d^2 x^\mu}{d\tau^2} + \Gamma_{\rho\sigma}^\mu \frac{dx^\rho}{d\tau} \frac{dx^\sigma}{d\tau} = 0, \quad (\text{A20})$$

in the limit $D_1 \rightarrow +\infty$ we obtain geodesics given by the Eq. (20). For an arbitrary constant D_1 we obtain geodesics given by the Eq. (21).

B. Point group discretization

Given a space-time manifold endowed with symmetry described by a Lie group, the discretization of the background via lattice construction necessitates a systematic

procedure for connecting the continuous symmetries of the underlying geometry with the discrete symmetries inherent to the lattice. This correspondence imposes specific constraints on the parameters characterizing the Lie group.

In this appendix, we provide a detailed derivation of the results presented in Sec. III. The transformation specified in Eq. (17) defines the action of a group element on a point within the disk, and thus serves as a representative element of the discrete symmetry group, contingent upon the imposition of appropriate conditions. As established in point group theory, repeated application of a group element yields the identity transformation. Here, we focus on the construction of rotational analogues, paralleling those found in flat space. While point group symmetries in Euclidean space can also encompass reflections, the presence of reflection symmetry in the hyperbolic setting is highly sensitive to the choice of Schläfli symbols $\{p, q\}$. Since our aim is to accommodate arbitrary $\{p, q\}$ tessellations, our analysis is restricted to rotational symmetries at this stage.

Let θ_p denote the angle associated with p successive applications of the transformation in Eq. (75), and let $\bar{\theta}$ correspond to the angle for a single application, as in Eq. (72). We introduce the notation

$$a_p = e^{i\theta_p}, \quad a = e^{i\bar{\theta}}, \quad (\text{B1})$$

and then obtain a recurrence relation given by the Eq. (76), which can be rewritten as

$$a_p = a \frac{a_{p-1} + c\bar{c}_{p-1}}{1 + \bar{c}c_{p-1}a_{p-1}}. \quad (\text{B2})$$

The same can be done with the equations for c_p . Now we define a new series as

$$b_p \equiv a_p c_p, \quad (\text{B3})$$

with the condition $b_1 = ac$. These series can be also written as a recurrence relation,

$$b_p = a \frac{b_{p-1} + c}{1 + \bar{c}b_{p-1}}. \quad (\text{B4})$$

In order to solve this recurrence relation, we define another two set of series as $b_p = \frac{m_p}{n_p}$, so the relation becomes:

$$\frac{m_p}{n_p} = a \frac{m_{p-1} + cn_{p-1}}{n_{p-1} + \bar{c}m_{p-1}}, \quad (\text{B5})$$

where we can equate separately the numerator and the denominator from the left and right-hand side of the equation. This yields the difference equation

$$m_{p+1} - (a+1)m_p + a(1 - |c|^2)m_{p-1} = 0, \quad (\text{B6})$$

which can be solved by introducing the parameter λ as

$$\lambda^2 - (a+1)\lambda + a(1 - |c|^2) = 0. \quad (\text{B7})$$

The solution to this quadratic equation can be readily found

$$\lambda_{1/2} = \frac{a+1 \pm \sqrt{(a-1)^2 + 4a|c|^2}}{2}. \quad (\text{B8})$$

Now the general solution for the elements of two defined series':

$$m_p = A\lambda_1^p + B\lambda_2^p, \quad (\text{B9})$$

$$n_p = \frac{1}{ac} [A\lambda_1^p(\lambda_1 - a) + B\lambda_2^p(\lambda_2 - a)], \quad (\text{B10})$$

or the previously defined series' element:

$$b_p = ac \frac{\lambda_1^p - \lambda_2^p}{(\lambda_1 - a)\lambda_1^p - (\lambda_2 - a)\lambda_2^p}, \quad (\text{B11})$$

where A and B are arbitrary constants.

Since the p -time applied transformation is equivalent to the unit element of the group, the element of the series becomes zero, i.e. $b_p = 0$. This implies that $\lambda_1^p = \lambda_2^p$, and we obtain

$$\left(\frac{\lambda_1}{\lambda_2}\right)^p = 1 \iff \frac{\lambda_1}{\lambda_2} = e^{i\frac{2n\pi}{p}}, \quad n \in \mathbb{Z}, \quad (\text{B12})$$

which implies

$$\lambda_1^2 = \lambda_1 \lambda_2 e^{i\frac{2n\pi}{p}} = a(1 - |c|^2) e^{i\frac{2n\pi}{p}}, \quad (\text{B13})$$

$$\lambda_1^2 + \lambda_2^2 = 2a(1 - |c|^2) \cos\left(\frac{2n\pi}{p}\right). \quad (\text{B14})$$

By further transforming Eqs. (B13) and (B14), the condition on Lie group parameters given by Eq. (80) can be readily obtained.

C. Noncommutativity of translations

As discussed in Sec. IIIB, the translation operators in curved space-time generally do not commute, which distinguishes them from their flat space counterparts. In this section, we derive the explicit conditions under which the translation operators commute.

To elucidate this, consider the standard quantization procedure analogous to that leading to Bloch's theorem.

We begin by introducing a basis for the Hilbert space \mathcal{H} , denoted by $\{|z\rangle \mid z \in \text{solution}\}$. The translation operators are then defined as

$$T_m \stackrel{\text{def.}}{=} \sum_z |z\rangle \langle t_m z|. \quad (\text{C1})$$

Assuming the flat-space approach remains valid, the corresponding eigenvalue problem for these operators can be formulated as

$$T_m |\lambda_1, \dots, \lambda_{p/2}\rangle = e^{i\lambda_m} |\lambda_1, \dots, \lambda_{p/2}\rangle, \quad (\text{C2})$$

where the eigenvectors can be expressed as linear combinations of the basis vectors in Hilbert space,

$$|\lambda_1, \dots, \lambda_{p/2}\rangle = \sum_z a_{\lambda_1 \dots \lambda_{p/2}}(z) |z\rangle. \quad (\text{C3})$$

Our definition of the translation operator leads to the following equation:

$$T_m |z\rangle = |t_m^{-1} z\rangle. \quad (\text{C4})$$

The condition on the eigenvalue λ_m is given by:

$$a_{\lambda_1 \dots \lambda_{p/2}}(t_m z) = e^{i\lambda_m} a_{\lambda_1 \dots \lambda_{p/2}}(z). \quad (\text{C5})$$

Up to this point, our analysis has not encountered any specific obstacles arising from the curvature of the underlying space. However, in order to determine the eigenvalues λ_m , it is necessary to derive the commutation relations between two arbitrary translation operators:

$$[T_n, T_m] = \left[\sum_z |z\rangle \langle t_n z|, \sum_{z'} |z'\rangle \langle t_m z'| \right] \quad (\text{C6})$$

$$= \sum_z (|z\rangle \langle t_m t_n z| - |z\rangle \langle t_n t_m z|). \quad (\text{C7})$$

We therefore compute the commutator of two translation transformations acting on a coordinate z :

$$[t_n, t_m]z = t_n t_m z - t_m t_n z, \quad (\text{C8})$$

where t_n denote the transformations defined in Eq. (98). This expression can be recast as a rational function, $[t_n, t_m]z = \frac{G}{D}$. Commutativity of the translation transformations is achieved if $G = 0$ and $D \neq 0$, with explicit forms of G and D given by

$$G = 4 \left\{ x^3 \cos \frac{\pi}{p} (n-m) \left[\sin \frac{2\pi}{p} (n-m) \sin \frac{\pi}{p} (n+m) (z^2 - 1) + i \cos \frac{\pi}{p} (n+m) \sin \frac{2\pi}{p} (n-m) (z^2 + 1) \right] \right. \quad (\text{C9})$$

$$\left. + i z x^2 \sin \frac{2\pi}{p} (n-m) \left(1 + x^2 \cos \frac{2\pi}{p} (n-m) \right) \right\}, \quad (\text{C10})$$

$$D = \left(1 + 2zx e^{-i\frac{\pi}{p}(n+m)} \cos \frac{\pi}{p} (n-m) \right)^2 + x^2 \left[x^2 + 2 \cos \frac{2\pi}{p} (n-m) \left(1 + 2zx e^{i\frac{\pi}{p}(n+m)} \right) \right]. \quad (\text{C11})$$

From these results, it follows that the condition for commutativity of two translation operators reads

$$n - m = \frac{pk}{2}, \quad n, m \in \{0, \dots, p-1\}, \quad k \in \mathbb{Z}. \quad (\text{C12})$$

This condition is only satisfied when $n = m$, i.e., translation operators commute only with themselves. Commutativity of translation operators, implying one-dimensional irreducible representations of pure translations, is essential for the form of the Bloch's theorem in flat space. For further details on the generalization of the Bloch's theorem to hyperbolic crystals, see Refs. [26, 29].

D. Dirac equation in hyperbolic space

Here we will analyze spinor fields on expanded Poincaré disk defined by the metric in Eq. (46). We recall the Dirac equation (47) and choose local γ matrices as Pauli matrices:

$$\gamma^0 = i\sigma_z = \begin{pmatrix} i & 0 \\ 0 & -i \end{pmatrix}, \quad (\text{D1})$$

$$\gamma^1 = \sigma_x = \begin{pmatrix} 0 & 1 \\ 1 & 0 \end{pmatrix}, \quad (\text{D2})$$

$$\gamma^2 = \sigma_y = \begin{pmatrix} 0 & -i \\ i & 0 \end{pmatrix}, \quad (\text{D3})$$

with $\{\gamma_a, \gamma_b\} = 2\eta_{ab}$.

In order to find the Dirac equation (47) for the case of fermions on Poincaré disk, we need to find the helicity operator, vielbeins and the spin connection. The helicity operator can be found from formula $\Sigma_{ab} = \frac{1}{4}[\gamma_a, \gamma_b]$ and its components are given by:

$$\Sigma_{01} = \frac{1}{4}[\gamma_0, \gamma_1] = \frac{1}{2}\gamma_2, \quad (\text{D4})$$

$$\Sigma_{02} = \frac{1}{4}[\gamma_0, \gamma_2] = -\frac{1}{2}\gamma_1, \quad (\text{D5})$$

$$\Sigma_{12} = \frac{1}{4}[\gamma_1, \gamma_2] = -\frac{1}{2}\gamma_0. \quad (\text{D6})$$

Next, we introduce vielbeins to satisfy $G_{\mu\nu} = e_\mu^a e_\nu^b \eta_{ab}$, where η_{ab} is metric of the Minkowski spacetime. Thus, vielbeins are not uniquely defined. With that in mind, we choose them in the form

$$e_t^0 = 1, \quad e_x^1 = e_y^2 = \frac{1}{1 - \frac{x^2+y^2}{l^2}}. \quad (\text{D7})$$

Now, the components of the spin connection read [61]:

$$\omega_\mu^a{}_b = e_\nu^a e^\lambda{}_b \Gamma_{\mu\lambda}^\nu - e^\lambda{}_b \partial_\mu e_\lambda^a. \quad (\text{D8})$$

For our choice of vielbeins, we obtain the following non-zero spin connection coefficients,

$$\omega_x^1{}_2 = \frac{2y}{l^2} \frac{1}{1 - \frac{x^2+y^2}{l^2}}, \quad (\text{D9})$$

$$\omega_y^1{}_2 = -\frac{2x}{l^2} \frac{1}{1 - \frac{x^2+y^2}{l^2}}. \quad (\text{D10})$$

The Dirac equation (47) can now be rewritten as,

$$[i\sigma_z \partial_t + \left(1 - \frac{x^2+y^2}{l^2}\right)(\sigma_x \partial_x + \sigma_y \partial_y) + \frac{1}{l^2}(y\sigma_y + x\sigma_x) - m]\Psi = 0. \quad (\text{D11})$$

Note that by introducing the spin-connection term in the Dirac equation, the naive interpretation of Hamiltonian fails. We mention that from a quantum mechanical perspective, the concept of energy in this context becomes ambiguous and requires further interpretation, which is an issue we do not further consider here.

Our goal now is to find the stationary solution of Eq. (D11) and the corresponding wavefunctions for fermions.

An ansatz for stationary solution of the Dirac equation (D11) can be written as,

$$\Psi(t, x, y) = \begin{pmatrix} \phi(x, y) \\ \chi(x, y) \end{pmatrix} e^{-iEt}, \quad (\text{D12})$$

where E is energy-like quantity. Implementing the ansatz to Eq. (D11), we obtain

$$E\phi + \left(1 - \frac{x^2+y^2}{l^2}\right)(\partial_x - i\partial_y)\chi + \frac{1}{l^2}(x - iy)\chi - m\phi = 0, \quad (\text{D13})$$

$$-E\chi + \left(1 - \frac{x^2+y^2}{l^2}\right)(\partial_x + i\partial_y)\phi + \frac{1}{l^2}(x + iy)\phi - m\chi = 0. \quad (\text{D14})$$

It is more convenient to solve these equations in polar

coordinates with $\phi = R(r)F(\varphi)$ and use symmetry based

solution for $F(\varphi) = e^{in\varphi}$ to find

$$R''(r) + \frac{1}{r}R'(r) + \left[\frac{E^2 - m^2 + \frac{1}{l^2}}{(1 - \frac{r^2}{l^2})^2} + \frac{2n+1}{l^2(1 - \frac{r^2}{l^2})} - \frac{n^2}{r^2} \right] R(r) = 0. \quad (\text{D15})$$

The dimensional analysis implies that the third term in Eq. (D15) corresponds to a momentum-like quantity $\frac{l}{\hbar} \sqrt{\frac{E^2}{c^2} - m^2 c^2} = \frac{l}{\hbar c} \sqrt{p^2 c^2} = lk$, where $p = \hbar k$.

Now, we can write the solution for the free massive fermion on the Poincaré disk:

$$\psi_{n,k}^<(r, \varphi) = A_n(k) e^{in\varphi} r^n \begin{pmatrix} \left(1 - \frac{r^2}{l^2}\right)^{\frac{1}{2}(1-ilk)} {}_2F_1\left(-\frac{i}{2}lk + 1, -\frac{i}{2}lk - n; 1 - n; \frac{r^2}{l^2}\right) \\ \left(1 - \frac{r^2}{l^2}\right)^{\frac{1}{2}(1+ikl)} {}_2F_1\left(\frac{i}{2}kl, \frac{i}{2}kl - n + 1; 1 - n; \frac{r^2}{l^2}\right) \end{pmatrix}, n < 0 \quad (\text{D16})$$

$$\psi_{n,k}^>(r, \varphi) = B_n(k) e^{in\varphi} r^{-n} \begin{pmatrix} \left(1 - \frac{r^2}{l^2}\right)^{\frac{1}{2}(1-ilk)} {}_2F_1\left(-\frac{i}{2}lk, -\frac{i}{2}lk + n + 1; 1 + n; \frac{r^2}{l^2}\right) \\ \left(1 - \frac{r^2}{l^2}\right)^{\frac{1}{2}(1+ikl)} {}_2F_1\left(\frac{i}{2}kl + 1, \frac{i}{2}kl + n; n + 1; \frac{r^2}{l^2}\right) \end{pmatrix}, n \geq 0 \quad (\text{D17})$$

where $A_n(k)$ and $B_n(k)$ are normalization constants dependent on the curvature radius l and the quantum numbers n and k . When employing a Euclidean time coordinate, the appearance of the imaginary unit in terms such as kl is avoided.

Eq. (D15) corresponds to the first component of the eigenvalue problem for the Casimir operator in the coordinate representation, as found in Sec. II C. Similar steps can be performed for the second component. Consequently, the obtained spinor components denote the symmetry-adapted basis.

Notice that as we approach the edge of the Poincaré disk, $r \rightarrow l$, these wave functions approach zero. A general solution of the Dirac equation can be written in the symmetry-adapted basis as

$$\Psi(t, r, \varphi) = \int dk \sum_n \left(\alpha_n(k) \psi_{n,k} e^{-iE_k t} + \beta_n(k) \psi_{n,k}^* e^{iE_k t} \right), \quad (\text{D18})$$

where $\alpha_n(k)$ and $\beta_n(k)$ are the functions of the momentum-like quantity and the angular momentum.

1. Dirac equation in flat space

For completeness, we here consider the flat-space limit of the Dirac equation in the hyperbolic space. Since the scalar curvature of the expanded Poincaré disk is given

by

$$R = -\frac{8}{l^2}. \quad (\text{D19})$$

the curvature vanishes in the limit $l \rightarrow \infty$. Therefore, we can use this to find the flat space form of our equations and compare our results (Eq. (D18)) with well-known results in flat space.

First, let us consider the metric (46) we introduced in Sec. II C:

$$ds^2 = -c^2 dt^2 + \frac{dx^2 + dy^2}{\left(1 - \frac{x^2 + y^2}{l^2}\right)^2}, \quad (\text{D20})$$

when $l \rightarrow \infty$, we obtain the ordinary three dimensional Minkowski space.

The Dirac equation (D11), in the limit $l \rightarrow +\infty$ can be written in the form

$$[i\sigma_z \partial_t + (\sigma_x \partial_x + \sigma_y \partial_y) - m]\Psi = 0. \quad (\text{D21})$$

With the choice of γ matrices [Eqs. (D1)-(D3)], we find

$$(\gamma^\mu \partial_\mu - m)\Psi = 0, \quad (\text{D22})$$

which represents the Dirac equation in flat space. Let us now solve it by employing the same stationary ansatz (D12) yielding

$$(E + m)\phi + (\partial_x - i\partial_y)\chi = 0, \quad (\text{D23})$$

$$-(E - m)\chi + (\partial_x + i\partial_y)\phi = 0. \quad (\text{D24})$$

Separation of the variables for $\phi = R(r)F(\varphi)$ yields the solution for angular part as $F(\varphi) = e^{in\varphi}$, while the solution for function $R(r)$ is given by the Bessel function $J_n(kr)$, where $k = \sqrt{E^2 - m^2}$. Therefore, the solution for ϕ reads

$$\phi(r, \varphi) = C J_n(kr) e^{in\varphi}, \quad (\text{D25})$$

where C is the normalization constant. One can show that the hypergeometric function can be reduced to the Bessel function in this limit $l \rightarrow +\infty$.

E. Symmetries of the Dirac equation on the Poincaré disk

In this section, we present the detailed derivation of the transformation generators for the spinor field, as introduced in Sec. II C. The infinitesimal coordinate transformation $z' = z + \delta z$ given in Eq. (17) takes the form

$$z' = z + i\theta z + \bar{c}z^2 - c. \quad (\text{E1})$$

Expressing $c = c_1 + ic_2$ and $z = x + iy$, the corresponding transformations for the real coordinates x and y are

$$x' = x - \theta y + c_1(-1 + x^2 - y^2) + 2c_2xy, \quad (\text{E2})$$

$$y' = y + \theta x + c_2(-1 - x^2 + y^2) + 2c_1xy. \quad (\text{E3})$$

These expressions directly generalize the infinitesimal coordinate transformation given in Eq. (48). To determine the corresponding transformation generators for the Dirac field, we consider the covariance of the Dirac equation under these transformations:

$$[\gamma'^\mu(x') D'_\mu(x') - m] \Psi'(x') = 0, \quad (\text{E4})$$

where D_μ denotes the covariant derivative, defined as $D_\mu = \partial_\mu + \omega_\mu = \partial_\mu + \frac{1}{2}\omega_\mu^{ab}\Sigma_{ab}$, and $\gamma^\mu(x) = e^\mu_a(x)\gamma^a$. In Eq. (E4), Greek indices refer to both spatial and temporal coordinates; however, in the following, we focus on stationary solutions of the Dirac equation and accordingly restrict Greek indices to spatial components. The transformation law for the metric is given by the variation

$$\delta_0 g_{\mu\nu}(x) = 0. \quad (\text{E5})$$

We now express the total variation of the metric tensor as

$$\delta g_{\mu\nu}(x) = \delta x^\rho \partial_\rho (e_\mu^a(x) e_\nu^b(x)) \eta_{ab}, \quad (\text{E6})$$

where η_{ab} is the identity matrix, as we consider only spatial coordinates, and $e_\mu^{a'}(x) = e_\mu^a(x)$.

From this, the transformation laws for the spin connection and the γ -matrices follow as

$$\omega'_\mu(x) = \omega_\mu(x), \quad (\text{E7})$$

$$\gamma'^\mu(x) = \gamma^\mu(x). \quad (\text{E8})$$

The infinitesimal transformation of the covariant derivative can thus be written as

$$D'_\mu(x') = \partial'_\mu + \omega'_\mu(x') \quad (\text{E9})$$

$$= \frac{\partial x^\rho}{\partial x'^\mu} \partial_\rho + \omega_\mu(x) + \delta x^\rho \partial_\rho \omega_\mu(x), \quad (\text{E10})$$

and the γ -matrices transform as

$$\gamma'^\mu(x') = \gamma^\mu(x) + \delta x^\rho \partial_\rho \gamma^\mu(x). \quad (\text{E11})$$

Taking into account the transformation from Eq. 49, the spinor field transforms as

$$\Psi'(x') = \left[1 + \frac{1}{2} w^{\mu\nu} M_{\mu\nu} + c^\mu K_\mu \right] \Psi(x) + \delta x^\mu \partial_\mu \Psi(x). \quad (\text{E12})$$

Noting that the rotation parameter can be expressed as $w^{\mu\nu} = \theta \varepsilon^{\mu\nu}$, we introduce the shorthand notation $M^{(0)} \equiv \varepsilon^{\mu\nu} M_{\mu\nu}^{(0)}$ and $M^\rho \equiv \varepsilon^{\mu\nu} M_{\mu\nu}{}^\rho$. Applying these transformations to Eq. (E4), we obtain the following algebra of the generators:

$$[\gamma^\rho, M^\mu] = 0, \quad (\text{E13})$$

$$[\gamma^\rho, M^{(0)}] = M^\mu (\partial_\mu \gamma^\rho) - \gamma^\mu (\partial_\mu M^\rho), \quad (\text{E14})$$

$$[\gamma^\rho, K_\mu{}^\nu] = 0, \quad (\text{E15})$$

$$[\gamma^\rho, K_\mu^{(0)}] = K_\mu{}^\nu (\partial_\nu \gamma^\rho) - \gamma^\nu (\partial_\nu K_\mu{}^\rho). \quad (\text{E16})$$

Eqs. (E13) and (E15) confirm that M^μ and $K_\mu{}^\nu$ act purely as coordinate representations, as assumed. The Killing vectors derived in Eqs. (7), (8), and (9) correspond directly to these coordinate representations of the generators. Incorporating this identification into Eqs. (E14) and (E16) yields the explicit forms of the matrix components of the transformation generators:

$$K_x^{(0)} = iy\sigma_z, \quad (\text{E17})$$

$$M = i\frac{\sigma_z}{2}, \quad (\text{E18})$$

$$K_y^{(0)} = -ix\sigma_z. \quad (\text{E19})$$

It can then be readily checked that the obtained generators satisfy the algebra of the Killing vectors from Eqs. (13)-(15).

F. Parallel transport method for discrete spin connection

We now outline an alternative method for deriving the discrete spin connection based on directly solving the parallel transport equation. As established in Sec. II A, the Poincaré disk admits two types of geodesics: straight lines passing through the disk's center [Eq. (20)] and orthogonal circles [Eq. (21)]. Parallel transport along the straight-line geodesics can be readily analyzed, analogously to the Euclidean case but with the normalization

condition imposed by the Poincaré disk metric. In contrast, for geodesics corresponding to orthogonal circles, the parallel transport equation must be solved explicitly, as detailed below. To simplify the calculation, we solve parallel transport equation along the geodesics in polar coordinates which read

$$\frac{dV^r}{dt} + \Gamma_{\varphi\varphi}^r \frac{d\varphi}{dt} V^\varphi + \Gamma_{rr}^r \frac{dr}{dt} V^r = 0, \quad (\text{F1})$$

$$\frac{dV^\varphi}{dt} + \Gamma_{r\varphi}^\varphi \left(\frac{dr}{dt} V^\varphi + \frac{d\varphi}{dt} V^r \right) = 0, \quad (\text{F2})$$

with Christoffel symbols also in polar coordinates. Non-zero Christoffel symbols obtained in the chosen model of hyperbolic space are given as

$$\Gamma_{\varphi\varphi}^r = -r \frac{r^2 + 1}{1 - r^2}, \quad (\text{F3})$$

$$\Gamma_{r\varphi}^\varphi = \frac{1}{r} \frac{r^2 + 1}{1 - r^2}, \quad (\text{F4})$$

$$\Gamma_{rr}^r = \frac{2r}{1 - r^2}, \quad (\text{F5})$$

where we have set $l = 1$. We proceed by simultaneously solving the parallel transport equations, Eqs. (F1) and (F2), and recasting them in a form that can be transformed into the equation of a circle. To facilitate this, we multiply each equation by an appropriate factor as fol-

lows:

$$\frac{dV^r}{dr} - r \frac{r^2 + 1}{1 - r^2} \frac{d\varphi}{dr} V^\varphi + \frac{2r}{1 - r^2} V^r = 0 \Big/ \cdot (1 - r^2)^{-1} \quad (\text{F6})$$

$$\frac{dV^\varphi}{dr} + \frac{1}{r} \frac{r^2 + 1}{1 - r^2} V^\varphi + \frac{1}{r} \frac{r^2 + 1}{1 - r^2} \frac{d\varphi}{dr} V^r = 0 \Big/ \cdot \frac{r}{1 - r^2} \quad (\text{F7})$$

This procedure reveals a symmetry between the equations, motivating the introduction of the variables:

$$\zeta^\varphi \equiv \frac{r}{1 - r^2} V^\varphi, \quad (\text{F8})$$

$$\zeta^r \equiv \frac{1}{1 - r^2} V^r. \quad (\text{F9})$$

After implementing expressions (F8) and (F9), and by summing the equations of parallel transport (F6) and (F7), we obtain

$$\frac{d}{dr} [(\zeta^\varphi)^2 + (\zeta^r)^2] = 0 \implies (\zeta^\varphi)^2 + (\zeta^r)^2 = a^2, \quad (\text{F10})$$

where a is an arbitrary constant. Solutions for defined vectors (Eqs. (F8) and (F9)) are now given by $\zeta^\varphi = a \cos \theta$ and $\zeta^r = a \sin \theta$. The differential equations for parallel transport (Eqs. (F1) and (F2)) can be rewritten as

$$\frac{d\theta}{dr} - \left(\frac{r^2 + 1}{1 - r^2} \right) \frac{d\varphi}{dr} = 0, \quad (\text{F11})$$

where we calculate $\frac{d\varphi}{dr}$ from the geodesic Eq. (21). We subsequently find

$$\frac{d\theta}{dr} = -\frac{\cot(\chi - \varphi)}{r}. \quad (\text{F12})$$

Here, there is the ambiguity of the sign of θ depending on the angle χ , which is defined as

$$\cos \chi = \frac{x_0}{\sqrt{x_0^2 + y_0^2}}, \quad \sin \chi = \frac{y_0}{\sqrt{x_0^2 + y_0^2}}. \quad (\text{F13})$$

Taking this into account, we can now integrate the Eq. (F12), yielding the form of angle θ as

$$\theta = \mp \frac{1}{2} \left[\arcsin \frac{\frac{1}{r^2} + 1 - 2(x_0^2 + y_0^2)}{2\sqrt{(x_0^2 + y_0^2)(x_0^2 + y_0^2 - 1)}} - \arcsin \frac{r^2 + 1 - 2(x_0^2 + y_0^2)}{2\sqrt{(x_0^2 + y_0^2)(x_0^2 + y_0^2 - 1)}} \right] + \theta_0, \quad (\text{F14})$$

where θ_0 is an integration constant, x_0 and y_0 are the coordinates of the center of the corresponding geodesic curve. From this we can readily write the vectors on the arbitrary site given by

$$V^r = \pm a \frac{1 - r^2}{2r\sqrt{R^2 + 1}} [\sqrt{4r^2(R^2 + 1) - (r^2 + 1)^2} \cos \theta_0 + (r^2 + 1) \sin \theta_0], \quad (\text{F15})$$

$$V^\varphi = \pm a \frac{1 - r^2}{2r^2\sqrt{R^2 + 1}} [(r^2 + 1) \cos \theta_0 - \sqrt{4r^2(R^2 + 1) - (r^2 + 1)^2} \sin \theta_0], \quad (\text{F16})$$

where a and θ_0 are integration constants, which determine the initial conditions of the vector being parallel transported, and R is the radius of the arbitrary geodesic curve from Eq. (21). The sign ambiguity comes from solving the parallel

transport equation, Eq. (F12). At last, having found the components of the parallel transported vectors, we express them in Cartesian coordinates.

Owing to symmetry, the difference between the angles of any two nearest sites of the central (zeroth generation) polygon is representative of all nearest-neighbor angle differences within that polygon. To find the angles θ_{ij} in this generation of polygons, arbitrary nearest-neighbor sites in the central polygon can be chosen, and for our analysis we again take the sites $D(r_0, -\frac{\pi}{p})$ and $B(r_0, \frac{\pi}{p})$ like in our other method presented in the main text, see Fig. 7. We set the vector we want to parallel transport from chosen site $B(r_0, \frac{\pi}{p})$, calculate the integration constant θ_0 that is adequate for corresponding geodesic curve and then use Eqs. (F15) and (F16). Depending on the chosen vector we obtain the spin connection angle θ_{ij} as

$$\theta_{ij} = \pm(\alpha_i - \beta_j) \quad (\text{F17})$$

where sign ambiguity comes from choosing the direction of parallel transport.

Angle θ , from Eq. (F14) in the zeroth generation takes values $\theta = \pm\beta + \theta_0 + n\frac{\pi}{2}$, where $n \in \mathbb{Z}$. By utilizing the result for the parallel transport equations Eq. (F15) and Eq. (F16) in Cartesian coordinates, we find

$$\mathbf{V}_B = \frac{a(1 - r_0^2)}{2r_0\sqrt{R^2 + 1}} \begin{pmatrix} \sqrt{4r_0^2(R^2 + 1) - (r_0^2 + 1)^2} \cos(\theta_0 - \frac{\pi}{p}) + (r_0^2 + 1) \sin(\theta_0 - \frac{\pi}{p}) \\ -\sqrt{4r_0^2(R^2 + 1) - (r_0^2 + 1)^2} \sin(\theta_0 - \frac{\pi}{p}) + (r_0^2 + 1) \cos(\theta_0 - \frac{\pi}{p}) \end{pmatrix}, \quad (\text{F18})$$

$$\mathbf{V}_M = \frac{a(1 - r_0^2)}{2r_0\sqrt{R^2 + 1}} \begin{pmatrix} \sqrt{4r_0^2(R^2 + 1) - (r_0^2 + 1)^2} \cos(\theta_0 - \frac{3\pi}{p}) + (r_0^2 + 1) \sin(\theta_0 - \frac{3\pi}{p}) \\ -\sqrt{4r_0^2(R^2 + 1) - (r_0^2 + 1)^2} \sin(\theta_0 - \frac{3\pi}{p}) + (r_0^2 + 1) \cos(\theta_0 - \frac{3\pi}{p}) \end{pmatrix}. \quad (\text{F19})$$

We choose to set the integration constant θ_0 to zero and obtain the angles α_i^{\parallel} and β_j^{\parallel} from the scalar product of the vectors, Eq. (111). Note that this scalar product should be calculated on the Poincaré disk as $\mathbf{V}_i \cdot \mathbf{V}_{r_i} = g_{\mu\nu} V_i^\mu V_{r_i}^\nu$, from which $\cos(\pm 2\alpha_i^g) \equiv \cos \theta_{ij}$ is readily calculated, yielding the result in Eq. (115).

It is important to note that, during parallel transport

within every generation, the geodesic connecting neighboring sites changes at each step, and this must be carefully accounted for in the procedure, i.e. one needs to recalculate the integration constants θ_0 and a at each step.

The method presented in this appendix is also used in accompanying Matlab code [68], for calculating the discrete spin connection in zeroth and first generation of polygons.

-
- [1] J. M. Maldacena, The large N limit of superconformal field theories and supergravity, *Int. J. Theor. Phys.* **38**, 1113 (1999).
 - [2] E. Witten, Anti-de Sitter space and holography, *Adv. Theor. Math. Phys.* **2**, 253 (1998).
 - [3] S. S. Gubser, I. R. Klebanov, and A. M. Polyakov, Gauge theory correlators from noncritical string theory, *Phys. Lett. B* **428**, 105 (1998).
 - [4] S. Ryu and T. Takayanagi, Holographic derivation of entanglement entropy from the anti-de sitter space/conformal field theory correspondence, *Phys. Rev. Lett.* **96**, 181602 (2006).
 - [5] S. Ryu and T. Takayanagi, Aspects of holographic entanglement entropy, *Journal of High Energy Physics* **2006**, 045 (2006).
 - [6] B. Swingle, Entanglement renormalization and holography, *Phys. Rev. D* **86**, 065007 (2012).
 - [7] B. Czech, L. Lamprou, S. McCandlish, and J. Sully, Integral geometry and holography, *Journal of High Energy Physics* **2015**, 175 (2015).
 - [8] T. Nishioka, Entanglement entropy: Holography and renormalization group, *Rev. Mod. Phys.* **90**, 035007 (2018).
 - [9] U. Leonhardt and T. G. Philbin, General relativity in electrical engineering, *New Journal of Physics* **8**, 247–247 (2006).
 - [10] S. Batz and U. Peschel, Linear and nonlinear optics in curved space, *Phys. Rev. A* **78**, 043821 (2008).
 - [11] I. I. Smolyaninov and E. E. Narimanov, Metric signature transitions in optical metamaterials, *Phys. Rev. Lett.* **105**, 067402 (2010).
 - [12] D. Genov, S. Zhang, and X. Zhang, Mimicking celestial mechanics in metamaterials, *Nature Physics* **5** (2009).
 - [13] H. Chen, R.-X. Miao, and M. Li, Transformation optics that mimics the system outside a schwarzschild black hole, *Optics Express* **18**, 15183 (2010).
 - [14] R. Bekenstein, Y. Kabessa, Y. Sharabi, O. Tal, N. Engheta, G. Eisenstein, A. Agranat, and M. Segev, Control of light by curved space in nanophotonic structures, *Nature Photonics* **11** (2017).
 - [15] R. Bekenstein, R. Schley, M. Mutzafi, C. Rotschild, and M. Segev, Optical simulations of gravitational effects in the newton-schrödinger system, *Nature Physics* **11** (2015).
 - [16] C. Sabín, Mapping curved spacetimes into dirac spinors, *Scientific Reports* **7**, 40346 (2017).

- [17] J. S. Pedernales, M. Beau, S. M. Pittman, I. L. Egusquiza, L. Lamata, E. Solano, and A. del Campo, Dirac equation in $(1 + 1)$ -dimensional curved spacetime and the multiphoton quantum rabi model, *Phys. Rev. Lett.* **120**, 160403 (2018).
- [18] C. Koke, C. Noh, and D. G. Angelakis, Dirac equation in 2-dimensional curved spacetime, particle creation, and coupled waveguide arrays, *Annals of Physics* **374**, 162–178 (2016).
- [19] O. Boada, A. Celi, J. I. Latorre, and M. Lewenstein, Dirac equation for cold atoms in artificial curved spacetimes, *New Journal of Physics* **13**, 035002 (2011).
- [20] A. J. Kollár, M. Fitzpatrick, and A. A. Houck, Hyperbolic lattices in circuit quantum electrodynamics, *Nature* **571**, 45 (2019).
- [21] W. Zhang, H. Yuan, N. Sun, H. Sun, and X. Zhang, Observation of novel topological states in hyperbolic lattices, *Nature Communications* **13**, 2937 (2022).
- [22] P. M. Lenggenhager, A. Stegmaier, L. K. Upreti, T. Hofmann, T. Helbig, A. Vollhardt, M. Greiter, C. H. Lee, S. Imhof, H. Brand, T. Kießling, I. Boettcher, T. Neupert, R. Thomale, and T. Bzdušek, Simulating hyperbolic space on a circuit board, *Nature Communications* **13**, 4373 (2022).
- [23] W. Zhang, F. Di, X. Zheng, H. Sun, and X. Zhang, Hyperbolic band topology with non-trivial second chern numbers, *Nature Communications* **14**, 1083 (2023).
- [24] A. Chen, H. Brand, T. Helbig, T. Hofmann, S. Imhof, A. Fritzsche, T. Kießling, A. Stegmaier, L. K. Upreti, T. Neupert, T. Bzdušek, M. Greiter, R. Thomale, and I. Boettcher, Hyperbolic matter in electrical circuits with tunable complex phases, *Nature Communications* **14**, 622 (2023).
- [25] J. Maciejko and S. Rayan, Hyperbolic band theory, *Sci. Adv.* **7**, eabe9170 (2021).
- [26] I. Boettcher, A. V. Gorshkov, A. J. Kollár, J. Maciejko, S. Rayan, and R. Thomale, Crystallography of hyperbolic lattices, *Phys. Rev. B* **105**, 125118 (2022).
- [27] N. Cheng, F. Serafin, J. McInerney, Z. Rocklin, K. Sun, and X. Mao, Band theory and boundary modes of high-dimensional representations of infinite hyperbolic lattices, *Phys. Rev. Lett.* **129**, 088002 (2022).
- [28] E. Kienzle and S. Rayan, Hyperbolic band theory through higgs bundles, *Adv. Math.* **409**, 108664 (2022).
- [29] J. Maciejko and S. Rayan, Automorphic bloch theorems for hyperbolic lattices, *Proc. Natl. Acad. Sci. USA* **119**, e2116869119 (2022).
- [30] A. Attar and I. Boettcher, Selberg trace formula in hyperbolic band theory, *Phys. Rev. E* **106**, 034114 (2022).
- [31] T. Bzdušek and J. Maciejko, Flat bands and band-touching from real-space topology in hyperbolic lattices, *Phys. Rev. B* **106**, 155146 (2022).
- [32] S. Yu, X. Piao, and N. Park, Topological hyperbolic lattices, *Phys. Rev. Lett.* **125**, 053901 (2020).
- [33] D. M. Urwyler, P. M. Lenggenhager, I. Boettcher, R. Thomale, T. Neupert, and T. c. v. Bzdušek, Hyperbolic topological band insulators, *Phys. Rev. Lett.* **129**, 246402 (2022).
- [34] Z.-R. Liu, C.-B. Hua, T. Peng, and B. Zhou, Chern insulator in a hyperbolic lattice, *Phys. Rev. B* **105**, 245301 (2022).
- [35] W. Zhang, H. Yuan, N. Sun, H. Sun, and X. Zhang, Observation of novel topological states in hyperbolic lattices, *Nature Communications* **13**, 2937 (2022).
- [36] L. Huang, L. He, W. Zhang, H. Zhang, D. Liu, X. Feng, F. Liu, K. Cui, Y. Huang, W. Zhang, and X. Zhang, Hyperbolic photonic topological insulators, *Nature Communications* **15**, 1647 (2024).
- [37] Q. Chen, Z. Zhang, H. Qin, A. Bossart, Y. Yang, H. Chen, and R. Fleury, Anomalous and chern topological waves in hyperbolic networks, *Nature Communications* **15**, 2293 (2024).
- [38] C. Sun, A. Chen, T. Bzdušek, and J. Maciejko, Topological linear response of hyperbolic Chern insulators, *SciPost Phys.* **17**, 124 (2024).
- [39] Y.-L. Tao and Y. Xu, Higher-order topological hyperbolic lattices, *Phys. Rev. B* **107**, 184201 (2023).
- [40] J. Sun, C.-A. Li, S. Feng, and H. Guo, Hybrid higher-order skin-topological effect in hyperbolic lattices, *Phys. Rev. B* **108**, 075122 (2023).
- [41] T. Tummuru, A. Chen, P. M. Lenggenhager, T. Neupert, J. Maciejko, and T. Bzdušek, Hyperbolic Non-Abelian Semimetal, *Phys. Rev. Lett.* **132**, 206601 (2024).
- [42] B. Roy, Magnetic catalysis in weakly interacting hyperbolic dirac materials, *Phys. Rev. B* **110**, 245117 (2024).
- [43] K. Ikeda, S. Aoki, and Y. Matsuki, Hyperbolic band theory under magnetic field and dirac cones on a higher genus surface, *Journal of Physics: Condensed Matter* **33**, 485602 (2021).
- [44] A. Stegmaier, L. K. Upreti, R. Thomale, and I. Boettcher, Universality of hofstadter butterflies on hyperbolic lattices, *Physical Review Letters* **128**, 10.1103/physrevlett.128.166402 (2022).
- [45] A. J. Kollár, M. Fitzpatrick, P. Sarnak, and A. A. Houck, Line-graph lattices: Euclidean and non-euclidean flat bands, and implementations in circuit quantum electrodynamics, *Communications in Mathematical Physics* **376**, 1909–1956 (2019).
- [46] A. Saa, E. Miranda, and F. Rouxinol, Higher-dimensional euclidean and non-euclidean structures in planar circuit quantum electrodynamics (2021), arXiv:2108.08854 [quant-ph].
- [47] T. c. v. Bzdušek and J. Maciejko, Flat bands and band-touching from real-space topology in hyperbolic lattices, *Phys. Rev. B* **106**, 155146 (2022).
- [48] R. Mosseri, R. Vogeler, and J. Vidal, Aharonov-bohm cages, flat bands, and gap labeling in hyperbolic tilings, *Phys. Rev. B* **106**, 155120 (2022).
- [49] X. Zhu, J. Guo, N. P. Breuckmann, H. Guo, and S. Feng, Quantum phase transitions of interacting bosons on hyperbolic lattices, *Journal of Physics: Condensed Matter* **33**, 335602 (2021).
- [50] P. Bienias, I. Boettcher, R. Belyansky, A. J. Kollár, and A. V. Gorshkov, Circuit quantum electrodynamics in hyperbolic space: From photon bound states to frustrated spin models, *Phys. Rev. Lett.* **128**, 013601 (2022).
- [51] N. Gluscevic, A. Samanta, S. Manna, and B. Roy, Dynamic mass generation on two-dimensional electronic hyperbolic lattices, *Phys. Rev. B* **111**, L121108 (2025).
- [52] C. A. Leong and B. Roy, Non-hermitian catalysis of density-wave orders on euclidean and hyperbolic lattices (2025), arXiv:2501.18591 [cond-mat.str-el].
- [53] C. Lv, R. Zhang, Z. Zhai, and Q. Zhou, Curving the space by non-hermiticity, *Nature Communications* **13**, 2184 (2022).
- [54] M. Hu, J. Lin, and K. Ding, Unveiling non-hermitian spectral topology in hyperbolic lattices with non-abelian translation symmetry (2024), arXiv:2412.05607 [cond-]

- mat.mes-hall].
- [55] R. Shen, W. J. Chan, and C. H. Lee, Non-hermitian skin effect along hyperbolic geodesics, *Phys. Rev. B* **111**, 045420 (2025).
 - [56] H. Yan, Hyperbolic fracton model, subsystem symmetry, and holography, *Phys. Rev. B* **99**, 155126 (2019).
 - [57] H. Yan, K. Slagle, and A. H. Nevidomskyy, Y-cube model and fractal structure of subdimensional particles on hyperbolic lattices (2022), arXiv:2211.15829 [quant-ph].
 - [58] D. R. Brill and J. A. Wheeler, Interaction of neutrinos and gravitational fields, *Rev. Mod. Phys.* **29**, 465 (1957).
 - [59] T. Inagaki, T. Muta, and S. D. Odintsov, Dynamical symmetry breaking in curved spacetime, *Progress of Theoretical Physics Supplement* **127**, 93 (1997), <https://academic.oup.com/ptps/article-pdf/doi/10.1143/PTP.127.93/5160221/127-93.pdf>.
 - [60] R. C. Brower, E. S. Weinberg, G. T. Fleming, A. D. Gasbarro, T. G. Raben, and C.-I. Tan, Lattice dirac fermions on a simplicial riemannian manifold, *Phys. Rev. D* **95**, 114510 (2017).
 - [61] M. Blagojevic, *Gravitation and Gauge Symmetries* (CRC Press, 2001).
 - [62] I. Boettcher, P. Bienias, R. Belyansky, A. J. Kollár, and A. V. Gorshkov, Quantum simulation of hyperbolic space with circuit quantum electrodynamics: From graphs to geometry, *Phys. Rev. A* **102**, 032208 (2020).
 - [63] A. Kitaev, Notes on $\widetilde{\mathfrak{sl}}(2, \mathbb{R})$ representations (2018), arXiv:1711.08169 [hep-th].
 - [64] S. T. Bishop C., Representation theoretic rigidity in $\mathrm{PSL}(2, \mathbb{R})$, *Acta Math.* **170**, 121 (1993).
 - [65] R. Camporesi, The Spinor heat kernel in maximally symmetric spaces, *Commun. Math. Phys.* **148**, 283 (1992).
 - [66] E. Gorbar and V. Gusynin, Gap generation for dirac fermions on lobachevsky plane in a magnetic field, *Annals of Physics* **323**, 2132 (2008).
 - [67] H. J. Rothe, *Lattice Gauge Theories: An Introduction*, 4th ed. (World Scientific, 2012).
 - [68] A. Djordjevic, Discrete spin connection (2025).
 - [69] S. Sorella and E. Tosatti, Semi-metal-insulator transition of the hubbard model in the honeycomb lattice, *Europhysics Letters* **19**, 699 (1992).
 - [70] F. F. Assaad and I. F. Herbut, Pinning the order: The nature of quantum criticality in the hubbard model on honeycomb lattice, *Phys. Rev. X* **3**, 031010 (2013).
 - [71] Y. Otsuka, S. Yunoki, and S. Sorella, Universal quantum criticality in the metal-insulator transition of two-dimensional interacting dirac electrons, *Phys. Rev. X* **6**, 011029 (2016).
 - [72] C. L. Kane and E. J. Mele, Quantum spin hall effect in graphene, *Phys. Rev. Lett.* **95**, 226801 (2005).
 - [73] B. A. Bernevig, T. L. Hughes, and S.-C. Zhang, Quantum spin hall effect and topological phase transition in hgte quantum wells, *Science* **314**, 1757 (2006).
 - [74] M. Bañados, C. Teitelboim, and J. Zanelli, Black hole in three-dimensional spacetime, *Phys. Rev. Lett.* **69**, 1849 (1992).